UNIVERSITY OF OKLAHOMA

GRADUATE COLLEGE

MOISTURE EFFECTS ON DYNAMIC ELASTIC PROPERTIES OF SHALE FROM

DEEP FORMATIONS

A THESIS

SUBMITTED TO THE GRADUATE FACULATY

in partial fulfillment of the requirements for the

Degree of

MASTER OF SCIENCE

By

LEI HAN

Norman, Oklahoma

2018

MOISTURE EFFECTS ON DYNAMIC ELSTIC PROPERTIES OF SHALE FROM

DEEP FORMATIONS

A THESIS APPROVED FOR THE MEWBOURNE SCHOOL OF PETROLEUM

AND GEOLOGICAL ENGINEERING

BY

Dr. Ahmad Ghassemi, Chair

Dr. Xingru Wu

Dr. Mashhad Fahes

# Acknowledgements

I thank my advisor Dr. Ahmad Ghassemi for his help, support, and advice through my time at the University of Oklahoma. I have enjoyed my time working with him very much. His flexibility, enthusiasm and patience have made my time at OU valuable, successful and memorable.

I thank the members of my committee, Dr. Xingru Wu and Dr. Mashhad Fahes for donating their time and expertise to review and provide advice for my thesis work.

I thank Dr. Xuejun Zhou for donating his time to assist me while testing the rocks.

Finally, I thank the faculty and staff of the Mewbourne School of Petroleum and Geological Engineering for their hard work and contribution to my educations and many others.

# Table of Contents

# List of Tables

# List of Figures

# Abstract

Geomechanics testing is an important component of reservoir geomechanics studies for improving drilling, and stimulation operations. Usually the cores for geomechanical tests are exposed to non-native fluid and air prior to tests. Drilling experience and modeling work has shown that shales can be sensitive while exposed to water and air. Therefore, a good understanding of the impact of the exposure to atmosphere and fluids on the shale geomechanical properties is necessary. To understand the impact, a study was conducted to examine changes in shale characteristics because of exposure to different fluids. To facilitate investigation of this complex physico-chemical process, dynamic properties were used. Nine plugs including seven 1-inch diameter 2-inch long samples and two 4-inches diameter samples were cored from the Fluffy Kitten 16 State VDW 2 well. As shale can be susceptible to swelling and deterioration when exposed to non-native water, a new method was used to core the samples to minimize the impact of exposure. The coring process and the exposure time during the preparation process was carefully recorded.

After plug preparations, one sample was preserved in 7% KCl solution, one sample was preserved in decane, one sample was preserved in 11.5 lb/gal NaCl-based drilling mud, six samples including two 4-inches samples and four 1-inch samples were wrapped by cling wraps without using any fluids for perservation. Dynamic measurements were conducted on these two 4-inches samples and four 1-inch samples while they were taken out of the preservation condition under an axial load applied by the MTS (Material Test System) 810. Samples' weights, lab temperature and relative humidity were measured

before each test. After the test, the samples which were previously in a specific kind of fluid (KCl, decane, drilling fluid) were put back into preservation condition while the other air-dry samples were left in the room environment to get exposed. The weights of the samples increased due to the penetration of the preservation fluid through the pre-existing cracks while preserved in the fluids.  While the weights of samples which were preserved in fluids stabilized, they were taken out of the preservation fluids and were tested in the same way as the samples which were not contacted with any fluids as described above. The exposure time of these plugs to air and/or fluids during testing were recorded. The time intervals between two tests were gradually increased from 12 hours to 24 hours, and then 48 hours, 96 hours, etc., since the moisture change tends to be less active over time. Decane was used on some plugs, and since decane may have some impact on the rock dynamic properties, one sample was preserved in a jar full of decane to clarify its impact on shale samples. To determine the impact of drilling mud on the mechanical properties of shale which is crucial to well-stability, one 1-inch shale sample was preserved in a jar full of 11.5 lb/gal NaCl-based drilling mud. The change in dynamic mechanical properties was compared.

It was observed all the samples were losing weight because of the loss of the moisture at the start of exposure. However, their weights fluctuated with the change of relative humidity which determined whether the vapor pressure was bigger than the capillary pressure. The weight loss included two kinds of fluids for the samples which were previously preserved in the fluid (decane, drilling mud, KCl solution) during the exposure: 1. Fluids which entered the samples through the pre-existing cracks; 2. Free water in the

shale. P-wave velocity increased due to the absorption of preserving fluid as P-wave travels faster in liquid than in air. S-wave velocity was not affected by the absorption of preserving fluid since it cannot travel through liquid and air. It is also observed that P-wave velocity and S-wave velocity increased due to the contraction of samples with the loss of the native moisture content. The measured shale dynamic Young's modulus increased while losing moisture content without air trapped because of the suction pressure developed. While exposing for a longer time, fractures localized as the air pressure built up while it was trapped inside shale and due to the structure imbalance caused by the movement of moisture content as sudden drop of P-wave velocity, S-wave velocity, Young's modulus, Poisson's ratio were observed during exposure. The dynamic signal would be attenuated due to the growth of cracks. It would also significantly decrease due to the localization of fractures.

In this research, it provides evidence that the shale moisture content impacts its dynamic properties. The capillary pressure and vapor pressure equilibrium control shale moisture movement while is contacted with air. The absorption of moisture occurs while the vapor pressure is higher than the capillary pressure between the shale interlayers. The loss of moisture content will also happen while the capillary pressure is higher than the vapor pressure. Due to the loss of native moisture content if the exposure is not excessive, the attraction force between the interlayer will increase. On one hand, this force (if not excessive) can act as a confining effect which tends to strengthen the shale. On the other hand, this force will make shale shrink and can desiccate. Poisson's ratio did not show a major variation as the P-wave velocity and S-wave velocity increased at a similar rate due

to the contraction of shale during the loss of native moisture content at the start of exposure. The penetration of preserving fluid increased shale's dynamic Poisson's ratio. P-wave velocity increases if the absorption of preserving fluid happened as P-wave travels faster in liquid than in air. S-wave velocity is not affected by the absorption of preserving fluid since it cannot travel through liquid and air. If the exposure is excessive, the cracks will grow. The growth of the micro-cracks tends to attenuate dynamic signals. While exposure for a longer time causes fractures to localize due to the capillary pressure (air trapped inside shale due to the alteration of absorption and loss of moisture content). The formation of fractures significantly decreases the dynamic P-wave velocity and S-wave velocity.

# Chapter 1. Introduction

## 1.1 Introduction

As world conventional hydrocarbon resources have reduced rapidly in recent years, unconventional hydrocarbon resources are gradually taking the central stage in all phases of exploitation from exploration to production. Unconventional resources have played a very important role in the global energy and petroleum industry. The International Energy Agency (IEA) estimated that the volume of unconventional gas resources was around 380,000 billion cubic meters (Gm3), in which shale gas accounts for the biggest share of these resources (Unconventional Gas 2012). The increasing significance that shale gas plays has led to the need for a deeper understanding of shale behaviors.

Shale is a sedimentary rock formation which is generally composed of clay, quartz, and other minerals. Shale has extremely low permeability and complicated pore structures. Therefore, the technique of hydraulic fracturing and horizontal drilling are the keys to significantly improve the well productivity and economically produce these tight shale reservoirs. Shale is also a potential host media for high-level radioactive wastes. One of the most critical factors that affect hydraulic fracture propagation, wellbore stability, the productivity of a shale gas wells and the stability to bury radioactivity in deep formation shale is the rock-mechanical properties of shale.

Rock mechanical properties refer to the strength, elastic modulus, and Poisson's ratio, etc. which are important in petroleum engineering. The determination of a reservoir's mechanical properties is critical to reduce drilling risk and maximizing well and reservoir

productivity. Estimates of rock mechanical properties are essential to drilling programs, well stimulation, well placement, well completion design, exploration and production

When shales are retrieved from deep formations, it would take some time to transfer it from the field to the lab. In addition, shale rocks from deep formations have certain characteristics which make them difficult to handle correctly under laboratory conditions; these include the low permeability and high sensitivity to contacting fluids. When shale is contacted with non-native fluids its properties may be altered.

The objective of this research is to understand how the deep-buried organic-rich shale dynamic mechanical properties (such as Young's moduli and Poisson's ratios) respond during/after the sample preparation stage and after contacting with different kinds of fluids. This is to ascertain if strict preservation practices are needed before geomechanical testing. For this purpose, dynamic tests were conducted on shale samples to investigate their mechanical properties variations during this period (saturation/desaturation). An axial load is used to maintain good contacts between shale samples and platens. In order not to create mechanical damage in the samples during repeated tests, only a low axial (3MPa-5 MPa) load was applied when measuring dynamic properties. Different kinds of fluids were used to investigate their influence on shale's mechanical properties to determine a better way to preserve shale samples after they were retrieved. After contact with a given fluid for a certain time, the samples were taken out of the fluid and placed in the room environment to get exposed (temperature and relative humidity were

measured throughout the process). Each sample's dynamic mechanical properties were compared.

## 1.2 Literature Review

The water content in organic-rich shale only exists in the inorganic pore because kerogen is hydrophobic. Usually, a rock with a high content of organic matter has a lower water content. While in the pore without organic matters, the water will be attracted by the clay minerals as clay mineral is hydrophilic.

The moisture content in shale are usually generalized into three types: 1. Free water which exists as filling macro-pores (>10 µm) between clay aggregates and/or particles of accessory minerals as well as interparticle pores on the border of microns; 2. Bound water which occupies the interlayer spacing; 3. Crystalline water which is contained in the unit layer. The bound water and crystalline water are hard to remove than free water (Temperature above 100 ℃ is needed to remove bound water, temperature above 550 ℃ is necessary to remove crystalline water) (H. Santos).

Darley & Gray (1991) observed a higher potential for shale to swell if it is interacted with water-based solution. Experiments have been conducted to prove that the artifacts will be induced which causes shale to swell due to the dehydration of shale (Forsans & Schmitt, 1994; Schmitt et al., 1994; Onaisi et al., 1994)

Water content has a significant impact on the acoustic velocities measurement. Two kinds of physical activities during the desaturation process are considered: 1) the water move from the interlayers of rock to the surface; 2) the vaporization between the rock surface

and air. Elastic properties of rocks have been shown to be affected by water content. In most cases, the rock will become weaker and easier to fail if the water content increase. The phenomenon is usually referred to as a water weakening effect. Researchers have spent lots of time trying to quantify this kind of weakening effect on lots of rocks, however, it remained challenging. There are three major water weakening mechanisms which are chemical effects, water clay interaction and capillary pressure increase (B.T. Lai 2015). Meng et al. (2005) concluded that with increasing of the water content, the molecular activity also increased which could affect the rock strength.

Ahmad Ghorbani (2009) found out that both P velocity and S velocity increased during the desiccation process in the study of desiccation effects on the Callovo-Oxfordian argillite formation samples. While exposed to 2% KCl water with friction reducer added, the Young's modulus did decrease in the shale (Ola Akrad 2011).

It was found out that the opening and closing of the inter-layers space was due to the gain and loss of the water which was also the reason why shale volume changes (F. Valès, 2004). F. Valès (2004) developed an experiment to investigate the physical and mechanical propetrties as a function of water saturation. He concluded that the swelling of shale was due to the opening of inter-layers which may also represent privileged paths for moisture diffusion and water transfer. There are two types of water existed in the shale formation: (1) The water is in the macro-connected pores with low bonding energy. (2) The water is in the small non-connected pores or in the thin clayed layers. It was found out that deformations are quite insignificant for the saturation under 76% RH, the

compressional velocity in the direction which is perpendicular to the bedding plane decreased with the loss of fluid in the fracture because water increases sample density and makes P-wave propagation easier. He found that the loss of the moisture content between the interlayer of shale will strengthen the rock.

Frederic L. P. (2007) found out that the delayed strain which would result in rock failure was observed in underground structures. P wave velocity will be affected by the cracks formed in the direction which is perpendicular to the wave propagation direction. S wave velocity will be affected by the cracks in the direction which is parallel to the wave propagation. These meant that the P wave and S wave velocity would significantly be decreased if there's a fracture formed in the rock. He pointed out that P-wave velocity fell even faster when there were micro-cracks initiated than the increase of the pore numbers.

Nur and Simmons (1969) showed that the formation of the microcracks would attenuate the signal quality while the wave propagation speed stayed relatively stable. If a new fracture was localized, the signal quality would be significantly attenuated, and the wave propagation speed would suddenly decrease.

In 1996, a regular spaced crack network developed on two galleries which were excavated perpendicular to the tunnel. The climatic conditions in the tunnel would affect the aperture of the cracks: The crack would close in a dry atmosphere (100% hygrometry). Nirina R. pointed out that this phenomenon suggests that higher tensile stresses got developed when the rock is submitted to desaturation.

Mikaël R. (2007) found out that the uniaxial compressive strength is affected by water. Chenevert (1970) postulated that the contraction exerts an overall confining pressure which strength the shale if no air could enter (increase both Young's modulus and compressive strength).

Well stability-related problems are crucial to determine whether a reservoir could be recovered economically. Most wells drilled would go through shale formations before they reached the reservoir (A. Onaisi, 1994). It is generally accepted by the industry that the well instability is mostly related to reaction between shale and drilling mud. The ion and water transfer between shale and drilling mud is believed to be the major reason why the well instability occurs while drilling through shale formation (A. Onaisi, 1994).

It is found that suction would get developed in the shale which is over-pressured due to the compaction. This suction pressure will act like a confining pressure which strengthen the shale. Also, air which was trapped inside the pore space generates tension which might break shales (A. Onaisi, 1994). The increase of strength while losing moisture content were also observed by Hale et al. (1993).

Schmitt et al. (1994) postulated that the increase of strength of shale while dehydrating might because of the pore contraction. While the compressibility of these pores cannot accommodate the water loss, the cracks would get developed. Greene-Kelly (1973) found that the surface tension forces would occur in the clay matrix which also contribute to the destructive reaction while drying in air.

The possibility of redistribution of water inside shale was pointed out by Mody &Hale (1993). While exposing to air, the outer part of shale lost moisture content first. The inner part would still stay wet. The moisture content tends to move from the higher saturation inner part to lower saturation outer part which induces the imbalance. The structure would be destroyed which leads to the formation of cracks due to this imbalance (H. Santos, 1997).

It is postulated that the idea to increase shale strength by dehydrating may cause serious side effects because micro-fracture could be induced in this process. The problems could overcome the benefits in all cases (H. Santos, 1997).

# Chapter 2. Sample preparation and characterization

To investigate the impact of moisture content on shale mechanical properties, cylindrical shale samples were prepared for tests. While shale was contacted with non-native fluids or air, its properties can be altered and may even break. The traditional coring method by using regular coring bit and water would increase the chances to change shale properties and might even break shale into pieces. Therefore, another way to minimize the exposure and reduce the risk to breaking shale is necessary. A new method was described below to core from shale which minimize the exposure to air and reduce the risk to breaking shales.

## 2.1 Sample preparation

Shale will swell if using the traditional coring method to core due to the contact with non-native fluid (water). Therefore, a new method was used to core 1-inch samples from 4-inches shale samples:

1. Shale was cut into an irregular shaped chunk whose diameter was close to 1-inch by using the band saw shown in Figure 1 with decane (the chunk was roughly a hexagonal shape). While cutting, the size of the chunk was monitored to be very close to 1-inch diameter cylinder to save time for step 2 to minimize the exposure time (the sample which was to be preserved in the KCl solution in the future was cut using KCl solution used as cooling fluid).

2. Grind the sides of the chunk until it became a cylinder by using the fixture device and grinding machine shown in Figure 2. During the grinding process, decane was

brushed on the surface of the samples to minimize the exposure to air and also to cool the band saw.

3. Cut the sample ends by using the band saw shown in Figure 1 to save time in polishing the two ends.

4. Use grinding machine to polish the two ends of the shale samples until they are flat (the difference between the two ends is less than 0.05 mm).

## 2.2 Sample preparation equipment and procedures

The band saw used to cut 4-inches shale into small chunks is shown in Figure 1. While cutting, the closer to 1-inch the diameter of shale chunks were, the better (please refer to section 3.2 for more details). The band saw shown in Figure 2 used has no teeth which makes the cutting process very gentle. Therefore, the risk to breaking the shale into pieces is significantly reduced during the cutting process. Decane and 7% KCl solution are used as cooling fluid while cutting. Decane is a good liquid to cool the band saw and lower the dynamic force and the vibrations between the shale and the saw without affecting the shale properties or alternating the shale mineralogical components.
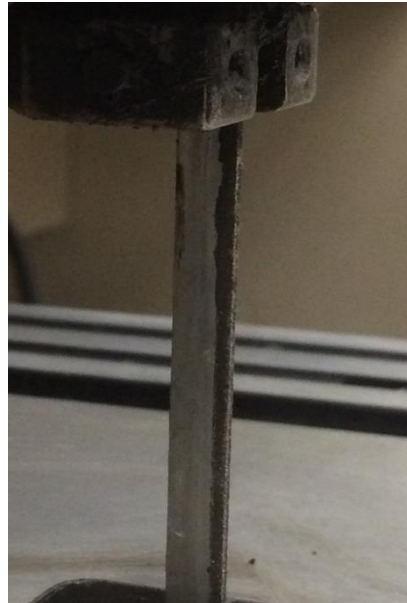
Figure 1 Band saw (it has no teeth)
used to cut shale into chunks

The fixture device and grinding machine used for grinding and polishing plugs into a cylinder are shown in Figure 2. The samples are fixed by holding two ends of shale samples with two small metal cones on the fixture. The fixture spins the sample in the direction opposite the sand-wheel spinning direction. By gradually lowering the height of the sand wheel, the sample is ground into a cylindrical geometry. The sample's diameter is measured after each round of grinding until the 1-inch diameter is reached. Samples' both ends will be polished to flat surfaces after they were ground into cylinders.
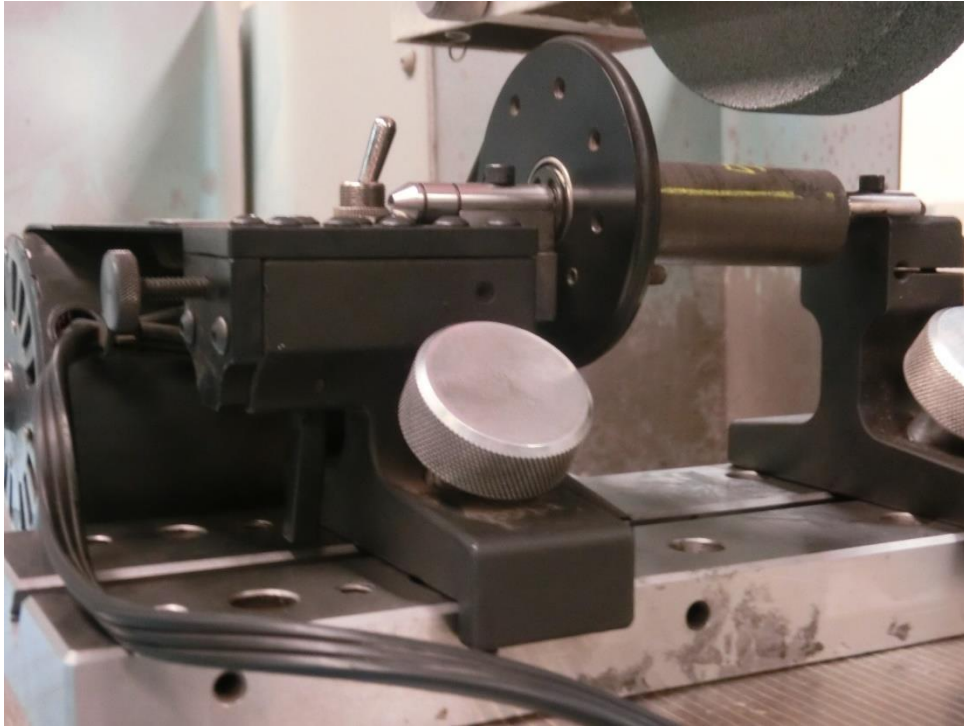
Figure 2 Fixture device and grinding machine used to polish sample to cylinder

## 2.3 Rock samples

Five 4-inches, 1 ft long plugs were cored from Fluffy Kitten 16 State VDW 2 well. They arrived carefully wrapped by using paraffin to prevent exposure right after they were taken out of the hole. Among them, two intervals which have the least cracks and higher clay content were selected to prepare the samples for the tests.

The CT scanning image and well log for the selected intervals (12,410ft-12,411ft and 12,389ft-12,390ft) are shown in Figure 3. From the well log plot and CT scanning mage,

many pre-existing fracture and cracks (cracks refer to a very tiny or incompletely separated fractures) were observed in the two intervals. The interval 12410ft-12411ft showed less pre-existing cracks than the interval 12389ft-12390ft.
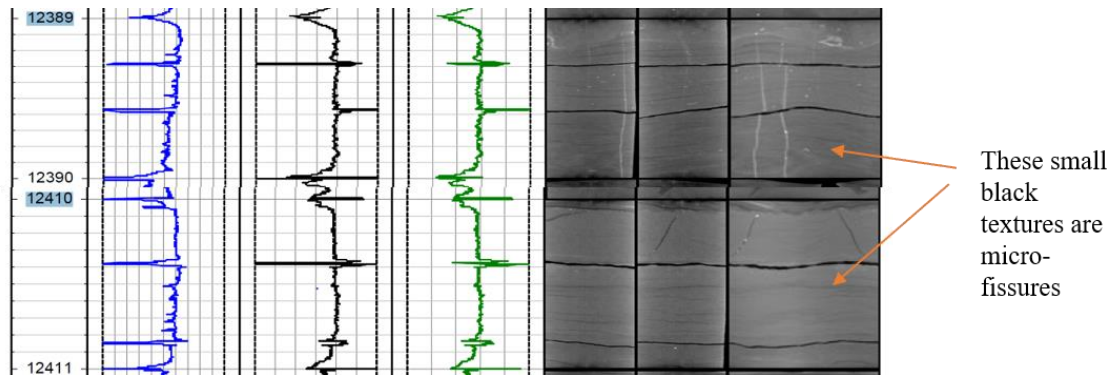


Figure 3. CT image and well log plot for interval 12410ft-12411ft and 12389ft-12390ft

In total, seven 1-inch samples were prepared. They are named as sample A, sample B, sample F, sample G, sample H, sample I and sample J.

Table 1 shows the depth interval which the samples were retrieved from and the volume percentage of clay mineral for sample A, B, D, E, F, G, H, I, J.

Table 1 The volume percentage of clay and depth information for each sample

| Sample | Interval (ft) | Vclay |
|---|---|---|
| A, B | 12389-12389.3 | 0.1595 |
| D | 12389.3-12389.6 | 0.1864 |
| E | 12389.6-12390 | 0.1707 |
| F, G, H, I, J | 12410.4-12410.8 | 0.1703 |

Sample A was cut and cored, and polished by using KCl solution (7%) as cooling fluid. Sample B, F, G, H, I, J were cut and cored by using decane as the cooling fluid. After polishing the ends, each sample was treated differently by using different kinds of preservation method before testing to determine the impact of different fluids on shale dynamic mechanical properties. The contacting fluid for each sample is shown in Table 2.

Table 2 Preservation method before test for each sample

| Sample | Preservation method before testing |
|---|---|
| A | Submerged in 7% KCl solution, then kept in the cooler after cylindrical sample was retrieved |
| B | Brushed with a thin layer of decane, wrapped with plastic wrap, then kept in the cooler after cylindrical sample was retrieved |
| D | Brushed with a thin layer of decane, wrapped with plastic wrap, then kept in the cooler after cylindrical sample was retrieved |
| E | Brushed with a thin layer of decane, wrapped with plastic wrap, then kept in the cooler after cylindrical sample was retrieved |
| F | NA (tested instantly after a cylindrical plug was retrieved) |
| G | Brushed with a thin layer of decane, wrapped with plastic wrap, then kept in the cooler after cylindrical sample was retrieved |
| H | Submerged in decane, then kept in the cooler after cylindrical sample was retrieved |
| I | Wrapped with plastic wrap, then kept in the cooler after cylindrical sample was retrieved |
| J | Wrapped with plastic wrap, then kept in the cooler after cylindrical sample was retrieved |

The exposure time due during the preparation process for sample A, B, D, E, F, G, H, I, J is 296 mins, 272 mins, 116 mins, 138 mins, 95 mins, 146 mins, 167 mins, 131 mins, 123 mins respectively.

Before testing, sample A was kept in the cooler for 552 hours while submerged in KCl solution. Sample B, D, E were kept in the preservation condition in the cooler for 547 hours, 526 hours, 846 hours respectively before being tested. Sample F was tested right after it became a plug. Sample G was kept in the preservation condition (see Table 2) in

13

the cooler for 20 mins before being tested. Sample G was brushed with a thin layer of decane, wrapped with cling wrap kept in the cooler for 20 mins. Then it was taken out of the cooler to be tested. Its weight was measured before & after applying a thin layer of decane and before the test. Sample H was brushed with a thin layer of decane. Its weight was measured before & after applying a thin layer of decane and before the test. The weight of sample G and H's during this process are shown in Table 3. After each dynamic test, all samples except H and J were left in open air to get exposed. Sample H was kept in a bottle full of decane for preservation then it was taken out to get exposed after 144 hours' preservation. Sample J was kept in a bottle full of 11.5 lb/gal NaCl-based drilling fluid. It was taken out of the mud to get exposed after 456 hours. The exposure and preservation time were also recorded.

Table 3 Sample G and H weights before & after brushing a thin layer of decane and before the test

| Process | weight (g) | |
|---|---|---|
| | G | H |
| Before applying decane | 50.11 | 58.11 |
| After applying decane | 50.14 | 58.17 |
| Before test | 50.12 | 58.13 |

Table 4 shows the time it took for sample coring for 1-inch samples A, B, F, G, H, I, J.

Table 4 1-inch Sample A, B, F, G, H, I, J exposure time and preservation time

| Process | Sample A | Sample B | Sample F | Sample G | Sample H | Sample I | Sample J |
|---|---|---|---|---|---|---|---|
| Cut shale into a chunk until its diameter is close to 1-inch (min) | 120 | 120 | 38 | 45 | 53 | 21 | 29 |
| Polish sides of the shale to cylinder (min) | 139 | 119 | 57 | 101 | 114 | 75 | 65 |
| Polish two ends of the cylinder (min) | 37 | 33 | | | | 35 | 29 |
| Preservation time before testing (hrs) | 552 | 547 | 0 | 20 mins | NA | 22 | 18 |

There were two 4-inches samples prepared which are named sample D and E. Both 4-inch samples were cut and polished. Both 4-inch samples' surfaces were brushed with a thin layer of decane. They were wrapped by using cling wrap then placed in the cooler for preservation. The time took for each process is recorded in Table 5.

Table 5 Sample D and sample E exposure time and preservation time

| Process | Sample D (thin layer decane applied) | Sample E (thin layer decane applied) |
|---|---|---|
| Cut ends of 4-inches sample to make it ready for polishing (mins) | 18 | 18 |
| Polishing both ends to flat (mins) | 98 | 120 |
| Preservation time by brushing decane, wrapping (hours) | 526 | 846 |

All the samples are shown in Figure 4.
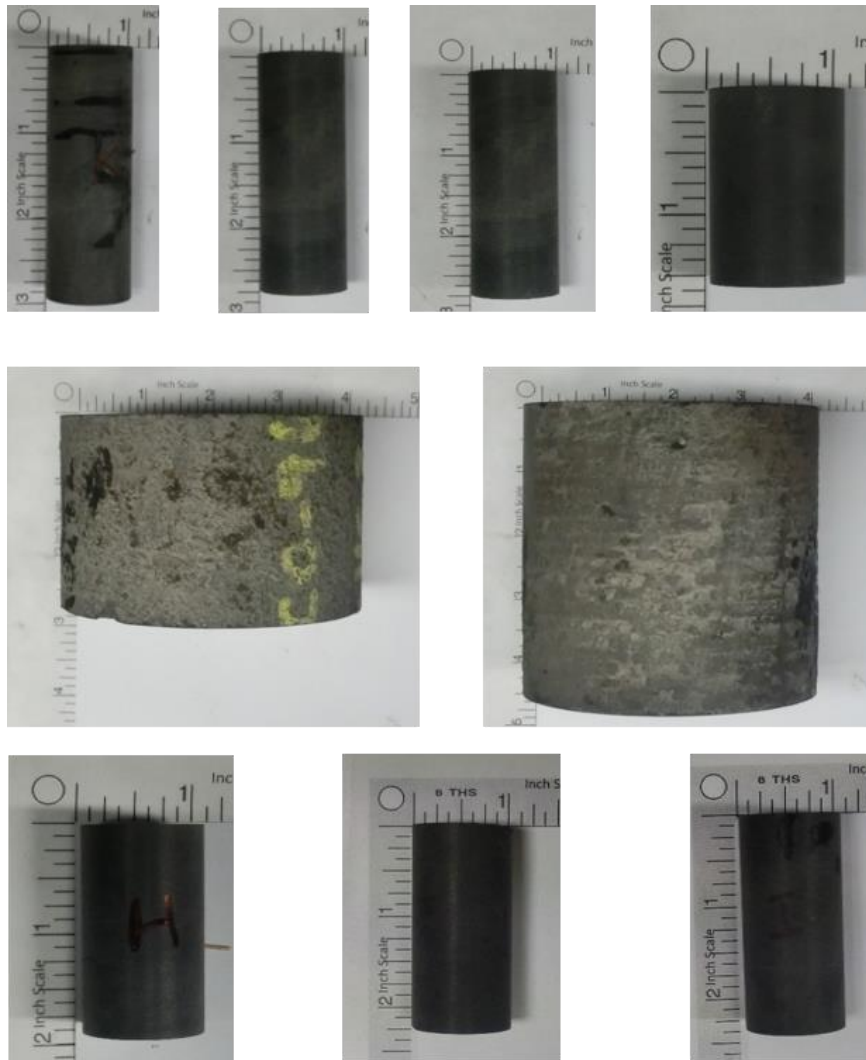


Figure 4 Sample A (first from upper left), Sample B(second from upper left), Sample D (middle left), Sample E (middle right), Sample F (third from upper left), Sample G (fourth from upper left), Sample H (bottom left), Sample I (bottom middle), Sample J (bottom right)

# Chapter 3. Experimental setup and configuration

## 3.1 Experimental setup

MTS 810 Material Test System is shown in Figure 5. It is used to apply the axial load to



Figure 5 MTS 810 Material
test system

guarantee a good contact between the platens and samples to minimize the attenuation of

the dynamic signal. A computer with MTS series $793^{TM}$ Controller software is used for

test control (maintain a stable axial load).

While running dynamic tests, the time taken for the wave to travel through steel platens was also included as the crystals are located in the platen. Therefore, a dynamic test on platen must be done before the formal test to obtain the delay effect of the platen on P-wave and S-wave velocity. To investigate the moisture effect on shale samples, dynamic tests were performed on seven 1-inch plugs and two 4-inches whole core after they were taken out of the preservation condition. An axial load was applied to ensure good contact between the platens and the sample. Before each test, the temperature and humidity were recorded for each sample.

The dynamic test equipment includes the followings:

1) HP 8116A Pulse/Function generator – create sine wave pulse shown in Figure 6.

2) Tektronix Mixed Domain Oscilloscope 3022 shown in figure 7– spot and record arrival time.

3) A computer with Tek OpenChoice Desktop software was used to record the waveform in both picture and excel format. Excitation frequencies:  250 kHz P and S crystals were used.

4) An Olympus voltage preamplifier.

Figure 6 HP 8116A Pulse/Function generator



Figure 7 Tektronix Mixed Domain Oscilloscope 3022

The 810 MTS test system configuration is shown in Figure 8.



Figure 8 Test system
configurations

The overall test configuration schematics is shown in Figure 9.
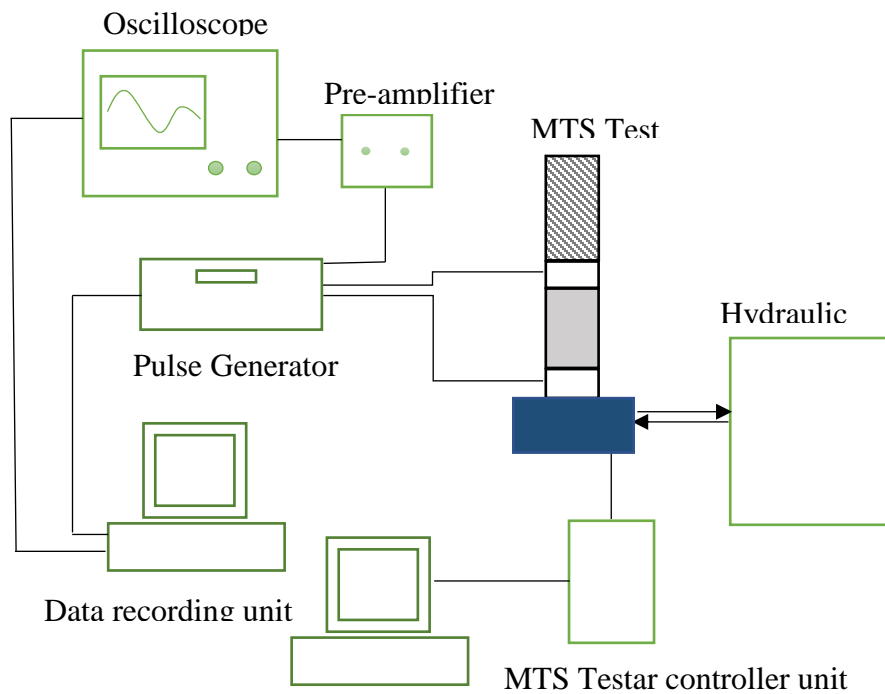


Figure 9 Overall test configuration schematics

## 3.2 Testing procedure for different sample groups

For the samples (A, B, D, E, F, F, G, I) which were tested only after they were taken out of the preservation condition shown in Table 1, the testing procedure is shown in Figure 10.
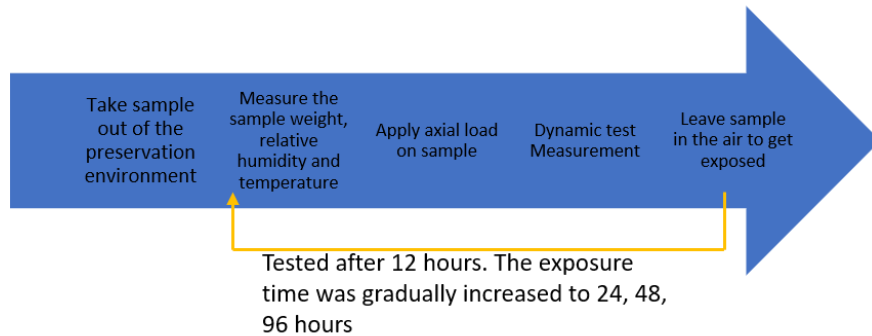


Figure 10 Testing procedure for samples which were tested only after they were taken out of the preservation condition

For the samples (H, J) which were tested while under preservation and after having been taken out of the preservation condition, the testing procedure is shown in Figure 11. The weights of each sample were plotted in terms of time. While seeing the change of weights are zero, the weights were treated as stable.
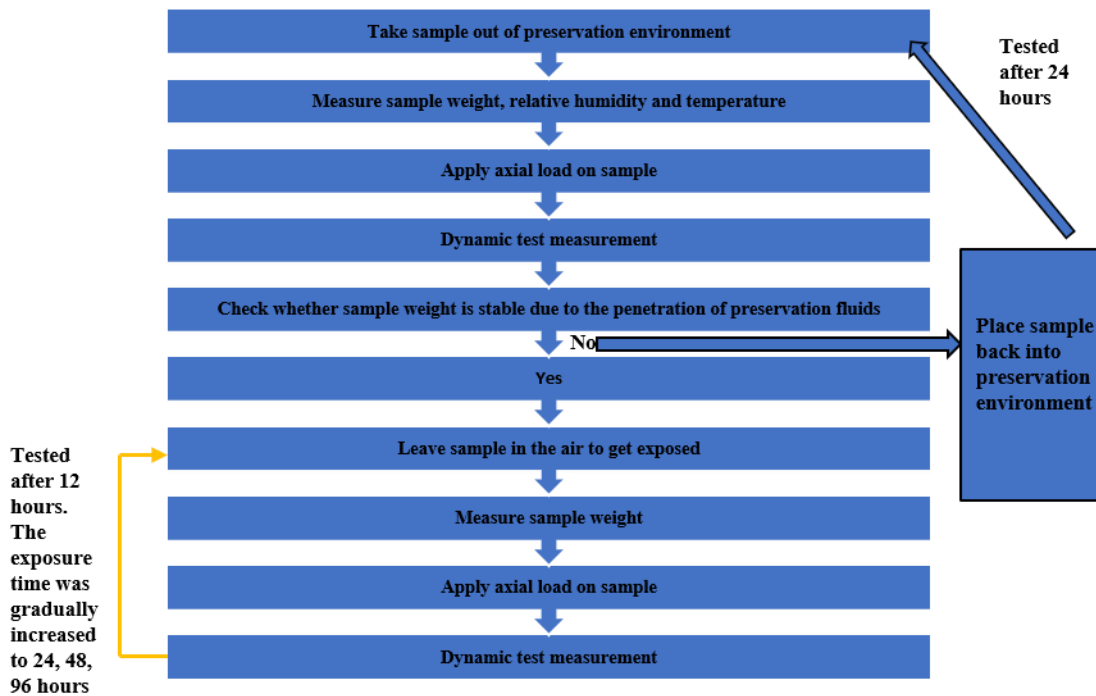
Figure 11 Testing procedure for samples which were tested while they were under preservation and after taken out of the preservation condition

An axial load of 435 psi (3MPa) was applied on sample A, B, D, F, G, H, I, J to make sure good contact between the sample and the platen. An axial load of 1015psi (7 MPa) were applied on sample E to make sure good contacts. Dynamic measurements in the horizontal direction were also conducted on sample D to observe how the dynamic properties will change with moisture loss in the horizontal direction.

# Chapter 4. Test results

## 4.1 Temperature and humidity record

Before testing samples A, B, D, F, G, H, I and sample J, the temperature and relative humidity were measured and recorded. The temperature and humidity changed with time during the test period were plotted in Figure 12. The temperature was almost constant around 22°C during this period while testing. The relative humidity change with time corresponded with the weather change. It would stay higher while raining (the relative humidity stayed low before and after raining for one day or two then increased if the weather became sunny) and remained lower while the weather was sunny. It can be observed that the relative humidity fluctuated quite often during the testing period.
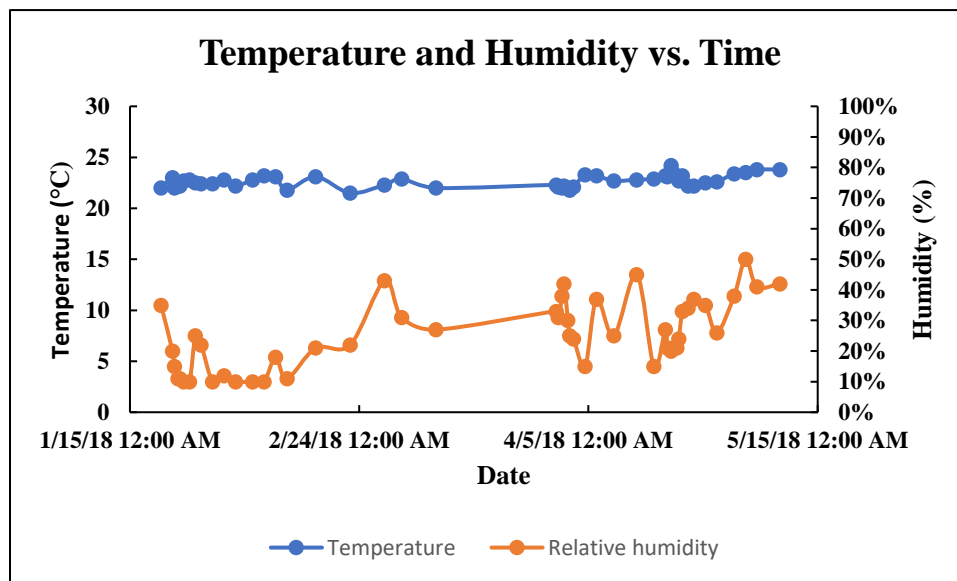
Figure 12 Change of temperature and humidity over time

The date to start to test each sample is shown in Table 6. By using the exposure time in the later chapter, we can know how the elastic dynamic properties is related to the relative humidity change.

Table 6 Tests starting date for each sample

| Sample | Test start date |
|--------|-----------------|
| A | 22-Jan |
| B | 22-Jan |
| D | 22-Jan |
| E | 2-Jan |
| F | 30-Jan |
| G | 1-Feb |
| H | 2-Feb |
| I | 10-Mar |
| J | 10-Mar |

## 4.2 Sample weight change

The weights and dimensions of samples A, B, D, E, F, G, H, I, J were measured before each test to quantify the moisture content change. It was observed that sample A, B, D, E, F, G and I lost weight while the room relative humidity was low. They also absorbed moisture content while the room relative humidity was high. Sample H and J's weights behaved differently from the other 1-inch samples as they were preserved in the decane and 11.5 lb/gal NaCl-based drilling mud respectively for some time. Their weights increased while in the fluid due to the penetration of the fluids through the pre-existing cracks. Then, after they were taken out of the preserving fluids to get exposed in the room

environment, their weight started to decrease due to moisture loss (native moisture and preservation fluids). The error analysis for the weight measurement is shown in Appendix.

Sample A's weight and dimension is shown in Table 6.

Table 7 Sample A's weight and dimension data

| No | Time (hour) | weight (g) | Length (mm) | Diameter | Density (g/cm^3) |
|---|---|---|---|---|---|
| 1 | 0 | 92.19 | 70.86 | 25.36 | 2.58 |
| 2 | 12 | 91.76 | 70.86 | 25.36 | 2.56 |
| 3 | 24 | 91.59 | 70.86 | 25.36 | 2.56 |
| 4 | 36 | 91.49 | 70.86 | 25.36 | 2.56 |
| 5 | 48 | 91.39 | 70.86 | 25.36 | 2.55 |
| 6 | 72 | 91.36 | 70.86 | 25.36 | 2.55 |
| 7 | 96 | 91.26 | 70.82 | 25.36 | 2.55 |
| 8 | 120 | 91.22 | 70.80 | 25.36 | 2.55 |
| 9 | 168 | 91.14 | 70.80 | 25.36 | 2.55 |
| 10 | 216 | 91.08 | 70.80 | 25.36 | 2.55 |
| 11 | 264 | 91.04 | 70.80 | 25.36 | 2.55 |
| 12 | 336 | 91.01 | 70.80 | 25.36 | 2.54 |
| 13 | 384 | 90.99 | 70.80 | 25.36 | 2.54 |
| 14 | 432 | 90.98 | 70.80 | 25.36 | 2.54 |
| 15 | 480 | 90.97 | 70.80 | 25.36 | 2.54 |
| 16 | 600 | 91.03 | 70.80 | 25.36 | 2.55 |
| 17 | 744 | 91.02 | 70.80 | 25.36 | 2.55 |
| 18 | 888 | 91.08 | 70.80 | 25.36 | 2.55 |
| 19 | 960 | 91.03 | 70.80 | 25.36 | 2.55 |
| 20 | 1104 | 90.98 | 70.80 | 25.36 | 2.54 |

Sample B's weight and dimension is shown in Table 7.

Table 8 Sample B's weight and dimension data

| No | Time (hour) | weight (g) | Length (mm) | Diameter | Density |
|----|-------------|-----------|-------------|----------|---------|
| 1 | 0 | 86.37 | 66.40 | 25.40 | 2.57 |
| 2 | 12 | 86.19 | 66.40 | 25.40 | 2.56 |
| 3 | 24 | 86.10 | 66.40 | 25.40 | 2.56 |
| 4 | 36 | 86.06 | 66.40 | 25.40 | 2.56 |
| 5 | 48 | 86.01 | 66.40 | 25.40 | 2.56 |
| 6 | 72 | 85.95 | 66.40 | 25.40 | 2.55 |
| 7 | 96 | 85.92 | 66.40 | 25.40 | 2.55 |
| 8 | 120 | 85.89 | 66.39 | 25.40 | 2.55 |
| 9 | 168 | 85.79 | 66.39 | 25.40 | 2.55 |
| 10 | 216 | 85.77 | 66.39 | 25.40 | 2.55 |
| 11 | 264 | 85.73 | 66.39 | 25.40 | 2.55 |
| 12 | 336 | 85.69 | 66.39 | 25.40 | 2.55 |
| 13 | 384 | 85.66 | 66.39 | 25.40 | 2.55 |
| 14 | 432 | 85.65 | 66.39 | 25.40 | 2.55 |
| 15 | 480 | 85.64 | 66.39 | 25.40 | 2.55 |
| 16 | 600 | 85.69 | 66.39 | 25.40 | 2.55 |
| 17 | 744 | 85.68 | 66.39 | 25.40 | 2.55 |
| 18 | 888 | 85.73 | 66.39 | 25.40 | 2.55 |
| 19 | 960 | 85.69 | 66.39 | 25.40 | 2.55 |
| 20 | 1104 | 85.64 | 66.39 | 25.40 | 2.55 |

Sample D's weight and dimension is shown in Table 8.

Table 9 Sample D's weight and dimension data

| No | Time (hour) | weight (g) | Length (mm) | Diameter (mm) | Density (g/cm^3) |
|----|-------------|-----------|-------------|---------------|-------------------|
| 1 | 0 | 1180.84 | 59.12 | 100.08 | 2.54 |
| 2 | 12 | 1179.80 | 59.12 | 100.08 | 2.54 |
| 3 | 24 | 1179.21 | 59.12 | 100.08 | 2.54 |
| 4 | 36 | 1178.88 | 59.12 | 100.08 | 2.53 |
| 5 | 48 | 1178.48 | 59.12 | 100.08 | 2.53 |
| 6 | 72 | 1178.00 | 59.12 | 100.08 | 2.53 |
| 7 | 96 | 1177.59 | 59.12 | 100.08 | 2.53 |
| 8 | 120 | 1177.36 | 59.12 | 100.08 | 2.53 |
| 9 | 168 | 1176.80 | 59.12 | 100.08 | 2.53 |
| 10 | 216 | 1176.40 | 59.12 | 100.08 | 2.53 |
| 11 | 264 | 1175.99 | 59.12 | 100.08 | 2.53 |
| 12 | 336 | 1175.42 | 59.12 | 100.08 | 2.53 |
| 13 | 408 | 1175.16 | 59.12 | 100.08 | 2.53 |
| 14 | 456 | 1174.98 | 59.12 | 100.08 | 2.53 |
| 15 | 504 | 1174.72 | 59.12 | 100.08 | 2.53 |
| 16 | 624 | 1174.60 | 59.12 | 100.08 | 2.53 |
| 17 | 768 | 1174.17 | 59.12 | 100.08 | 2.52 |
| 18 | 912 | 1174.06 | 59.12 | 100.08 | 2.52 |
| 19 | 984 | 1173.78 | 59.12 | 100.08 | 2.52 |
| 20 | 1128 | 1173.37 | 59.12 | 100.08 | 2.52 |

Sample E's weight and dimension is shown in Table 9.

Table 10 Sample E's weight and dimension data

| No | Time (hour) | weight (g) | Length (mm) | Diameter (mm) | Density (g/cm^3) |
|---|---|---|---|---|---|
| 1 | 0 | 2022.40 | 102.89 | 100.45 | 2.48 |
| 2 | 12 | 2021.20 | 102.89 | 100.45 | 2.48 |
| 3 | 24 | 2020.10 | 102.89 | 100.45 | 2.48 |
| 4 | 48 | 2019.50 | 102.89 | 100.45 | 2.48 |
| 5 | 60 | 2019.20 | 102.89 | 100.45 | 2.48 |
| 6 | 72 | 2018.30 | 102.89 | 100.45 | 2.48 |
| 7 | 96 | 2018.30 | 102.89 | 100.45 | 2.48 |
| 8 | 120 | 2018.30 | 102.89 | 100.45 | 2.48 |
| 9 | 144 | 2017.20 | 102.89 | 100.45 | 2.47 |
| 10 | 168 | 2016.90 | 102.89 | 100.45 | 2.47 |
| 11 | 240 | 2016.50 | 102.89 | 100.45 | 2.47 |
| 12 | 288 | 2016.30 | 102.89 | 100.45 | 2.47 |
| 13 | 360 | 2014.40 | 102.89 | 100.45 | 2.47 |
| 14 | 432 | 2014.10 | 102.89 | 100.45 | 2.47 |
| 15 | 480 | 2013.88 | 102.89 | 100.45 | 2.47 |
| 16 | 528 | 2013.17 | 102.89 | 100.45 | 2.47 |
| 17 | 600 | 2012.83 | 102.89 | 100.45 | 2.47 |
| 18 | 696 | 2012.10 | 102.89 | 100.45 | 2.47 |
| 19 | 768 | 2011.61 | 102.89 | 100.45 | 2.47 |
| 20 | 840 | 2011.11 | 102.89 | 100.45 | 2.47 |
| 21 | 936 | 2010.65 | 102.89 | 100.45 | 2.47 |
| 22 | 1056 | 2010.73 | 102.89 | 100.45 | 2.47 |
| 23 | 1200 | 2010.38 | 102.89 | 100.45 | 2.47 |
| 24 | 1344 | 2010.46 | 102.89 | 100.45 | 2.47 |
| 25 | 1416 | 2010.09 | 102.89 | 100.45 | 2.47 |
| 26 | 1560 | 2009.64 | 102.89 | 100.45 | 2.46 |

Sample F's weight and dimension is shown in Table 10.

Table 11 Sample F's weight and dimension data

| No | Time (hour) | weight (g) | Length (mm) | Diameter | Density |
|----|-------------|------------|-------------|----------|---------|
| 1 | 0 | 65.36 | 52.20 | 25.02 | 2.55 |
| 2 | 16 | 65.18 | 52.20 | 25.02 | 2.54 |
| 3 | 24 | 65.14 | 52.20 | 25.02 | 2.54 |
| 4 | 40 | 65.08 | 52.20 | 25.02 | 2.54 |
| 5 | 48 | 65.06 | 52.20 | 25.02 | 2.54 |
| 6 | 64 | 65.00 | 52.20 | 25.02 | 2.53 |
| 7 | 73 | 64.99 | 52.20 | 25.02 | 2.53 |
| 8 | 90 | 64.95 | 52.20 | 25.02 | 2.53 |
| 9 | 100 | 64.95 | 52.20 | 25.02 | 2.53 |
| 10 | 120 | 64.93 | 52.20 | 25.02 | 2.53 |
| 11 | 139 | 64.89 | 52.20 | 25.02 | 2.53 |
| 12 | 161 | 64.88 | 52.20 | 25.02 | 2.53 |
| 13 | 191 | 64.85 | 52.20 | 25.02 | 2.53 |
| 14 | 215 | 64.84 | 52.20 | 25.02 | 2.53 |
| 15 | 234 | 64.83 | 52.20 | 25.02 | 2.53 |
| 16 | 258 | 64.82 | 52.20 | 25.02 | 2.53 |
| 17 | 282 | 64.81 | 52.20 | 25.02 | 2.53 |
| 18 | 306 | 64.80 | 52.20 | 25.02 | 2.52 |
| 19 | 354 | 64.80 | 52.20 | 25.02 | 2.52 |
| 20 | 402 | 64.83 | 52.20 | 25.02 | 2.53 |
| 21 | 474 | 64.85 | 52.20 | 25.02 | 2.53 |
| 22 | 546 | 64.81 | 52.20 | 25.02 | 2.53 |
| 23 | 618 | 64.80 | 52.20 | 25.02 | 2.52 |
| 24 | 690 | 64.83 | 52.20 | 25.02 | 2.53 |
| 25 | 762 | 64.81 | 52.20 | 25.02 | 2.53 |
| 26 | 906 | 64.78 | 52.20 | 25.02 | 2.52 |

Sample G's weight and dimension is shown in Table 11.

Table 12 Sample G's weight and dimension data

| No | Time (hour) | weight (g) | Length (mm) | Diameter | Density |
|----|----|----|----|----|----|
| 1 | 0 | 50.12 | 37.95 | 25.49 | 2.59 |
| 2 | 16 | 49.96 | 37.95 | 25.49 | 2.58 |
| 3 | 25 | 49.92 | 37.95 | 25.49 | 2.58 |
| 4 | 42 | 49.88 | 37.95 | 25.49 | 2.58 |
| 5 | 52 | 49.86 | 37.95 | 25.49 | 2.57 |
| 6 | 71 | 49.84 | 37.95 | 25.49 | 2.57 |
| 7 | 89 | 49.80 | 37.95 | 25.49 | 2.57 |
| 8 | 112 | 49.77 | 37.95 | 25.49 | 2.57 |
| 9 | 142 | 49.75 | 37.95 | 25.49 | 2.57 |
| 10 | 166 | 49.73 | 37.95 | 25.49 | 2.57 |
| 11 | 185 | 49.73 | 37.95 | 25.49 | 2.57 |
| 12 | 209 | 49.72 | 37.95 | 25.49 | 2.57 |
| 13 | 233 | 49.72 | 37.95 | 25.49 | 2.57 |
| 14 | 257 | 49.69 | 37.95 | 25.49 | 2.57 |
| 15 | 305 | 49.69 | 37.95 | 25.49 | 2.57 |
| 16 | 353 | 49.71 | 37.95 | 25.49 | 2.57 |
| 17 | 425 | 49.71 | 37.95 | 25.49 | 2.57 |
| 18 | 497 | 49.69 | 37.95 | 25.49 | 2.57 |
| 19 | 569 | 49.68 | 37.95 | 25.49 | 2.57 |
| 20 | 641 | 49.70 | 37.95 | 25.49 | 2.57 |
| 21 | 713 | 49.68 | 37.95 | 25.49 | 2.57 |
| 22 | 857 | 49.66 | 37.95 | 25.49 | 2.56 |

Sample H's weight and dimension is shown in Table 12.

Table 13 Sample H's weight and dimension data

| No | Time (hour) | weight (g) | Length (mm) | Diameter | Density |
|----|----|----|----|----|----|
| 1 | 0 | 58.13 | 45.07 | 25.45 | 2.54 |
| 2 | 24 | 58.25 | 45.07 | 25.45 | 2.54 |
| 3 | 48 | 58.27 | 45.07 | 25.45 | 2.54 |
| 4 | 72 | 58.29 | 45.07 | 25.45 | 2.54 |
| 5 | 91 | 58.30 | 45.07 | 25.45 | 2.54 |
| 7 | 144 | 58.31 | 45.07 | 25.45 | 2.54 |
| 8 | 162 | 58.08 | 45.03 | 26.45 | 2.35 |
| 9 | 173 | 58.02 | 45.03 | 26.45 | 2.34 |
| 10 | 187 | 57.96 | 45.03 | 26.45 | 2.34 |
| 11 | 210 | 57.89 | 45.03 | 26.45 | 2.34 |
| 12 | 234 | 57.83 | 45.03 | 26.45 | 2.34 |
| 13 | 259 | 57.81 | 45.03 | 26.45 | 2.34 |
| 14 | 283 | 57.79 | 45.03 | 26.45 | 2.34 |
| 15 | 307 | 57.81 | 45.03 | 26.45 | 2.34 |
| 16 | 331 | 57.78 | 45.03 | 26.45 | 2.34 |
| 17 | 403 | 57.77 | 45.03 | 26.45 | 2.33 |
| 18 | 475 | 57.71 | 45.03 | 26.45 | 2.33 |
| 19 | 547 | 57.69 | 45.03 | 26.45 | 2.33 |
| 20 | 619 | 57.72 | 45.03 | 26.45 | 2.33 |
| 21 | 691 | 57.68 | 45.03 | 26.45 | 2.33 |
| 22 | 835 | 57.63 | 45.03 | 26.45 | 2.33 |

Sample I and sample J's weights and dimensions are shown in Table 13 and Table 14 respectively.

Table 14 Sample I's weight and dimension data

| No | Time (hour) | weight (g) | Length (mm) | Diameter | Density |
|----|------------|-----------|-------------|----------|---------|
| 1 | 0 | 71.75 | 56.07 | 25.34 | 2.54 |
| 2 | 12 | 71.58 | 56.07 | 25.34 | 2.53 |
| 3 | 24 | 71.51 | 56.07 | 25.34 | 2.53 |
| 4 | 36 | 71.50 | 56.07 | 25.34 | 2.53 |
| 5 | 48 | 71.44 | 56.07 | 25.34 | 2.53 |
| 6 | 60 | 71.40 | 56.07 | 25.34 | 2.53 |
| 7 | 72 | 71.36 | 56.07 | 25.34 | 2.52 |
| 8 | 120 | 71.28 | 56.07 | 25.34 | 2.52 |
| 10 | 168 | 71.26 | 56.07 | 25.34 | 2.52 |
| 11 | 240 | 71.18 | 56.07 | 25.34 | 2.52 |
| 12 | 336 | 71.23 | 56.07 | 25.34 | 2.52 |
| 13 | 408 | 71.12 | 56.07 | 25.34 | 2.52 |
| 14 | 456 | 71.15 | 56.07 | 25.34 | 2.52 |
| 15 | 468 | 71.13 | 56.07 | 25.34 | 2.52 |
| 16 | 480 | 71.12 | 56.07 | 25.34 | 2.52 |
| 17 | 492 | 71.11 | 56.07 | 25.34 | 2.51 |
| 18 | 504 | 71.11 | 56.07 | 25.34 | 2.51 |
| 19 | 516 | 71.11 | 56.07 | 25.34 | 2.51 |
| 20 | 540 | 71.13 | 56.07 | 25.34 | 2.52 |
| 21 | 564 | 71.13 | 56.07 | 25.34 | 2.52 |
| 22 | 588 | 71.14 | 56.07 | 25.34 | 2.52 |
| 23 | 636 | 71.16 | 56.07 | 25.34 | 2.52 |
| 24 | 684 | 71.14 | 56.07 | 25.34 | 2.52 |
| 25 | 756 | 71.16 | 56.07 | 25.34 | 2.52 |

Table 15 Sample J's weight and dimension data

| No | Time (hour) | weight (g) | Length (mm) | Diameter | Density |
|----|-------------|------------|-------------|----------|---------|
| 1 | 0 | 69.05 | 53.88 | 25.33 | 2.54 |
| 2 | 12 | 69.09 | 53.88 | 25.33 | 2.54 |
| 3 | 24 | 69.10 | 53.88 | 25.33 | 2.55 |
| 4 | 36 | 69.12 | 53.88 | 25.33 | 2.55 |
| 5 | 48 | 69.13 | 53.88 | 25.33 | 2.55 |
| 6 | 60 | 69.13 | 53.88 | 25.33 | 2.55 |
| 7 | 72 | 69.14 | 53.88 | 25.33 | 2.55 |
| 8 | 120 | 69.15 | 53.88 | 25.33 | 2.55 |
| 10 | 168 | 69.17 | 53.88 | 25.33 | 2.55 |
| 11 | 240 | 69.18 | 53.88 | 25.33 | 2.55 |
| 12 | 336 | 69.19 | 53.88 | 25.33 | 2.55 |
| 13 | 408 | 69.18 | 53.88 | 25.33 | 2.55 |
| 14 | 456 | 69.19 | 53.88 | 25.33 | 2.55 |
| 15 | 468 | 69.02 | 53.88 | 25.33 | 2.54 |
| 16 | 480 | 68.94 | 53.88 | 25.33 | 2.54 |
| 17 | 492 | 68.91 | 53.88 | 25.33 | 2.54 |
| 18 | 504 | 68.87 | 53.88 | 25.33 | 2.54 |
| 19 | 516 | 68.85 | 53.88 | 25.33 | 2.54 |
| 20 | 540 | 68.84 | 53.88 | 25.33 | 2.54 |
| 21 | 564 | 68.82 | 53.88 | 25.33 | 2.53 |
| 22 | 588 | 68.81 | 53.99 | 25.33 | 2.53 |
| 23 | 636 | 68.79 | 53.99 | 25.33 | 2.53 |
| 24 | 684 | 68.76 | 53.99 | 25.33 | 2.53 |
| 25 | 756 | 68.76 | 54.00 | 25.33 | 2.53 |

All the samples' weights are plotted in terms of the time they were exposed to compare

their weights' change throughout the test period. The change of sample A, B, D, E, F,

G, H, I, J's weights over exposure time is shown in Figure 13, 14, 15, 16, 17, 18, 19, 20,

21.

Figure 13 Change of sample A's weight over time

The weight of sample A was decreasing over time after exposing to air at the start due to the loss of moisture content. The rate of weight decrease is not uniform. The weight change at the start of exposure was very fast then slowed down over time. On Feb $11^{th}$, sample A's weight increased due to the higher relative humidity. The fluctuation of the weight can be observed (the weight of sample A increased for some time then decreased).

Figure 14 The change of sample B's weight over time

The weight of sample B was decreasing over time after it was exposed to air at the start due to the loss of moisture content. The weight decreasing rate is not uniform. The weight change at the start of exposure was very fast then slowed down over time. On Feb 11th, sample B's weight increased due to the higher relative humidity (20% relative humidity shown on Figure 12. Relative humidity was 10% before Feb 11th). The fluctuation of the weight can be observed (the weight of sample B increased for some time then decreased).

Figure 15 The change of sample D's weight over time

The weight of sample D was decreasing over time after exposing to air at the start due to the loss of moisture content. The weight decreasing rate is not uniform. The weight change at the start of exposure was very fast then slowed down over time. The moisture content would be first lost from the surface of the sample. Then the moisture content tends to move from the core part to the surface of the sample. For a bigger sample, this process would take a longer time. The losing process is not uniform. Therefore, when the relative humidity is high on Feb 11th, part of the surface showed loss of the native moisture, the other part which still has abundant moisture showed absorption of the moisture driven by the capillary pressure and vapor pressure. On Feb 11th, the weight loss of native moisture content was more than the weight absorption from the air. That is why sample D still showed weight loss without increasing around Feb 11th. However, we can still see the weight loss rate decreased due to this.
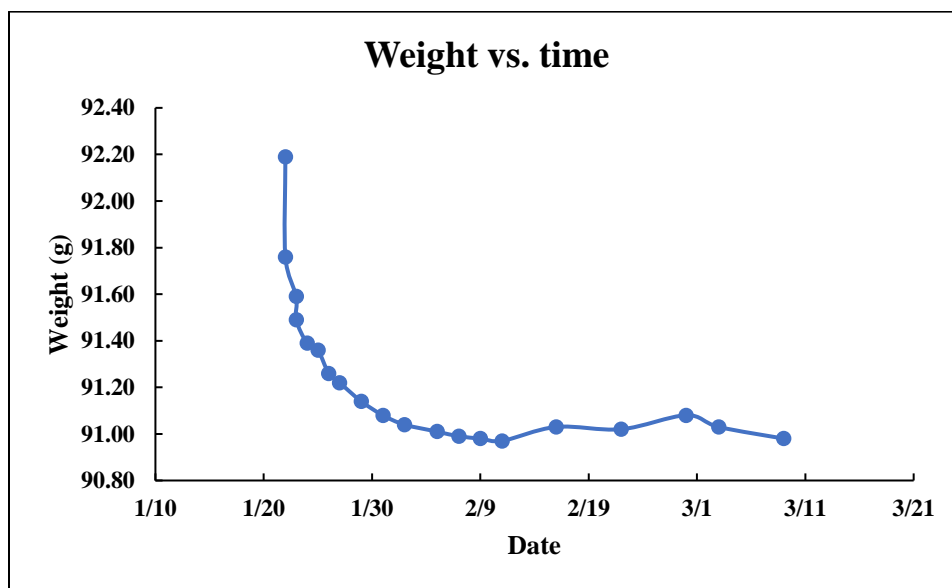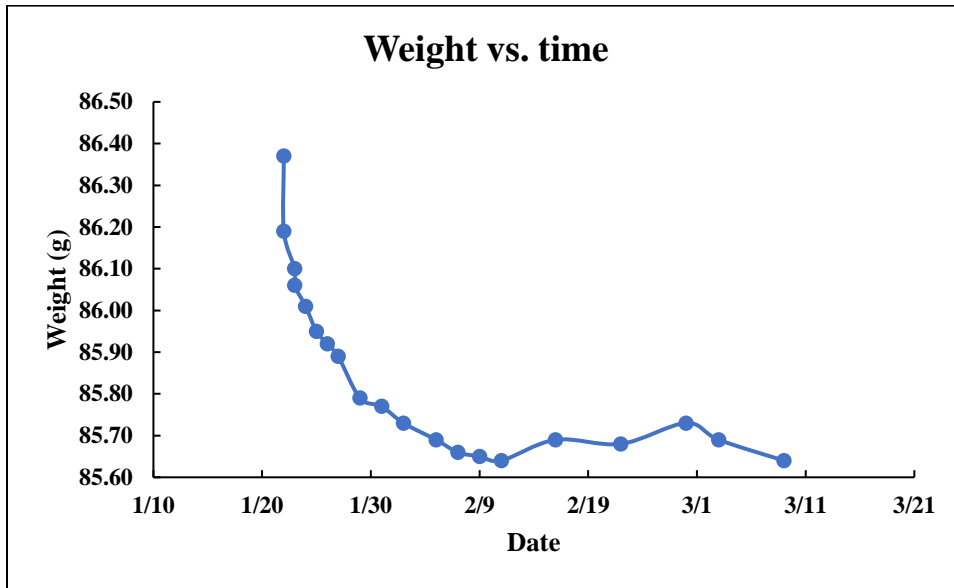
34

Figure 16 The change of sample E's weight over time

The weight of sample E was decreasing over time after exposing to air at the start due to the loss of moisture content. The weight decreasing rate is not uniform. The weight change at the start of exposure was very fast then slowed down over time. Similar as reason stated for sample D, while the relative humidity was high on Feb 11th, the loss of the native moisture content and the absorption of moisture both happened at the same time. The loss of native moisture content was more than the absorption of moisture from the air, sample E still showed weight loss. That's why from the data point on Jan 5th, 6th and 7th which has a higher relative humidity, we can see the weight of sample E stayed stable in these days. It can be observed that the weight declining rate (moisture loss rate) slowed down. This proved that both moisture content absorption and loss happened at the same time.

35
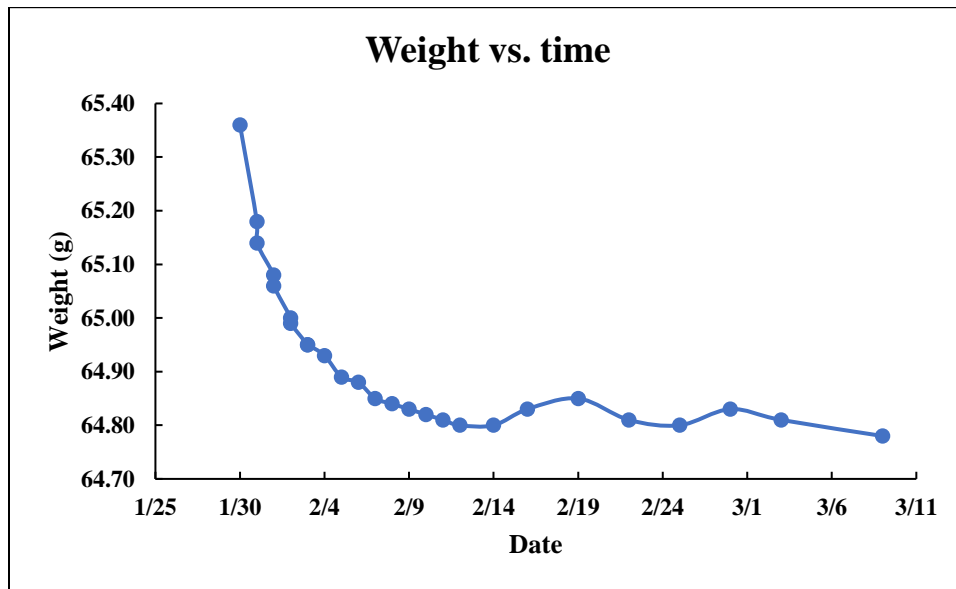
Figure 17 The change of sample F's weight over time

The weight of sample F was decreasing over time while exposed to air due to the loss of moisture content. The decreasing rate of weight is not uniform. The weight change at the start of exposure was very fast then slowed down over time. After Feb 11th, the sample F's weight began to fluctuate due to the loss and absorption of moisture content associated with the fluctuation of the relative humidity (It increased for some time then decreased).
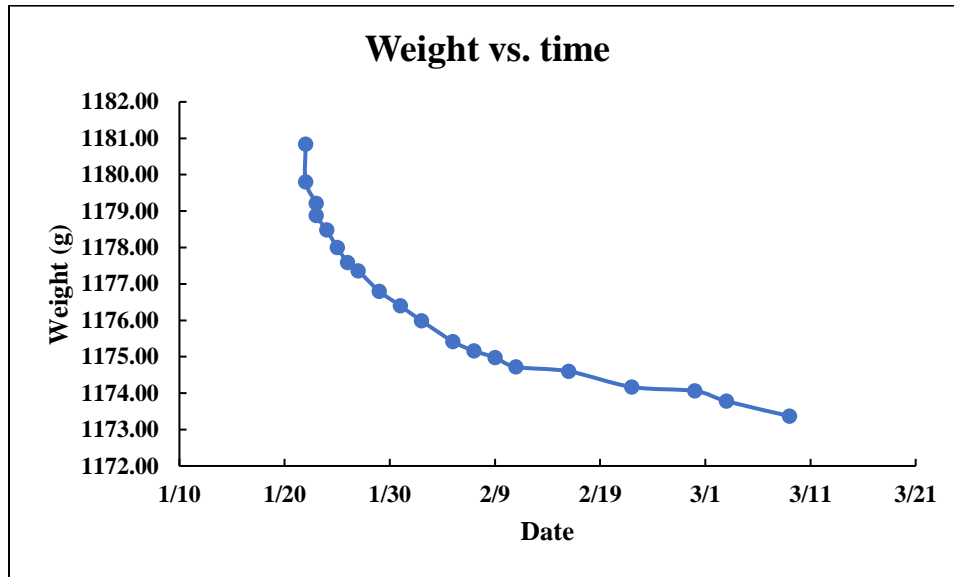
Figure 18 The change of Sample G's weight over time

The weight of sample G was decreasing over time while exposed to air due to the loss of moisture content. The decreasing rate of weight is not uniform. The weight change at the start of exposure was very fast then slowed down over time. After Feb 11$^{th}$, after about 257 hours, sample G's weight began to fluctuate due to the loss or absorption of moisture content associated with the fluctuation of the relative humidity (It increased for some time then decreased).

**Weight vs. time**
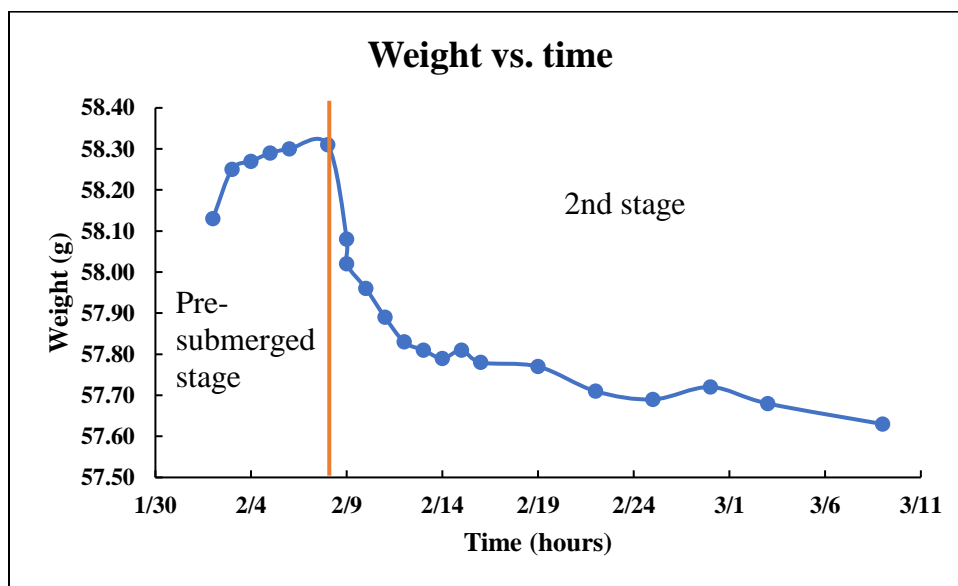
Figure 19 The change of sample H's weight over time

The weight of sample H was increasing at early time as it was preserved in the decane. The decane penetrated the sample through the pre-existing cracks. It increased very fast at first then stabilized. When it was taken out of the decane at around 144 hours, its weight began to decrease due to the exposure to air. The decreasing rate of weight is not uniform. The weight decreased at the start of exposure was very fast then slowed down over time. After Feb 24th, after about 547 hours, the fluctuation of the weight can be observed due to the loss or absorption of moisture content associated with the fluctuation of the relative humidity (the weight of sample H increased for some time then decreased).
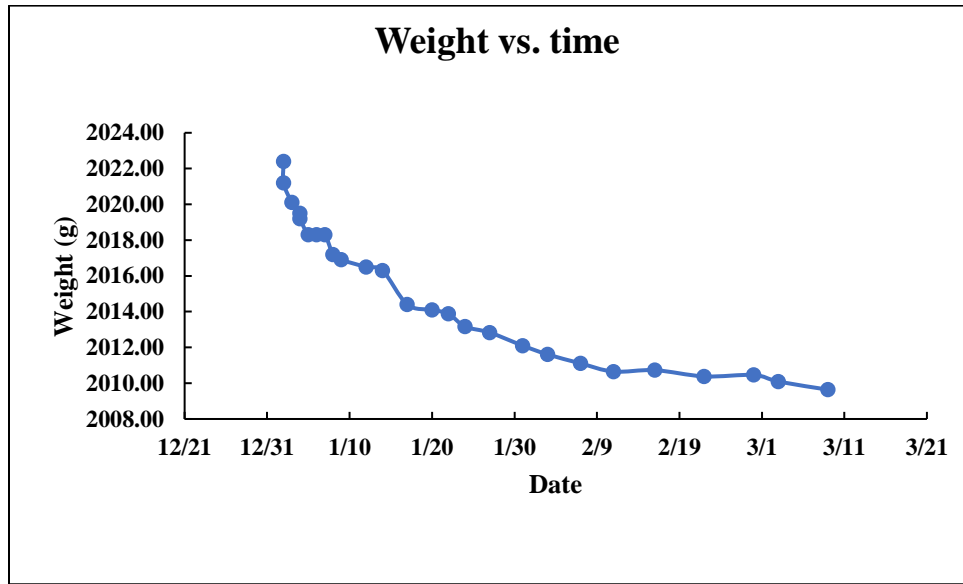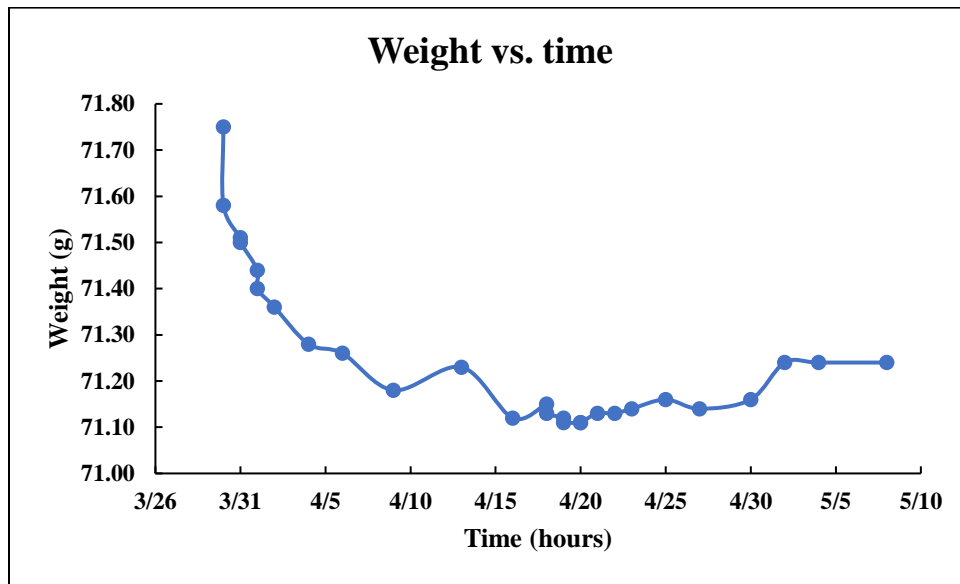
Figure 20 The change of sample I's weight over time

The weight of sample I was decreasing over time while exposed to air due to the loss of moisture content. The decreasing rate of weight is not uniform. The weight change at the start of exposure was very fast then slowed down over time. After about 257 hours, on April 9th, sample I's weight began to fluctuate due to the loss or absorption of moisture content associated with the fluctuation of the relative humidity (It increased for some time then decreased).
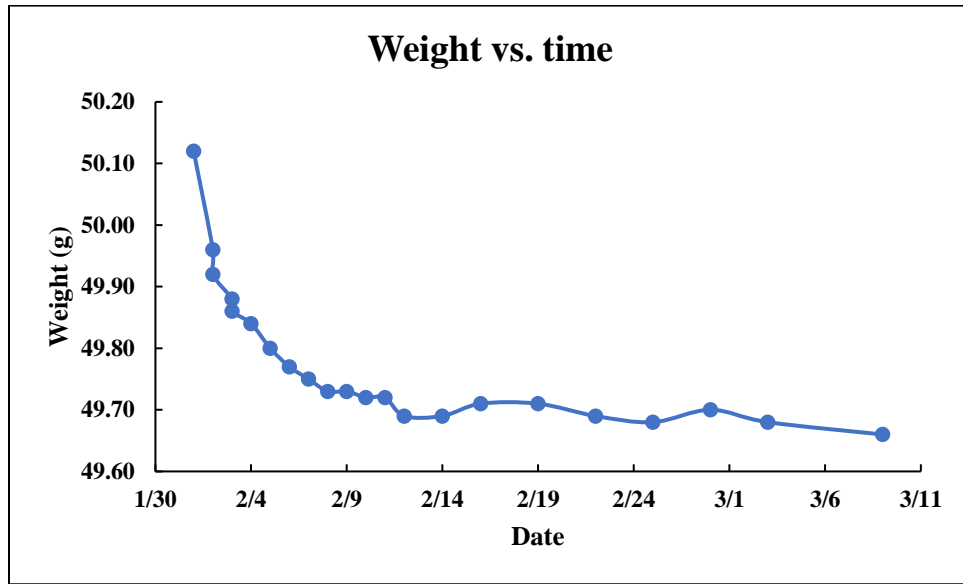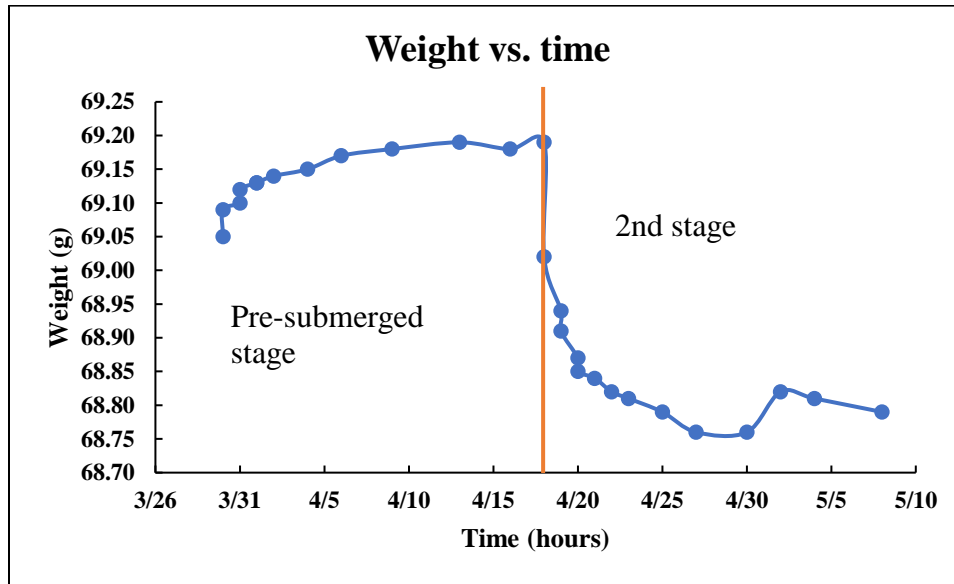
Figure 21 Change of sample J's weight over time

The weight of sample J was increasing at early time as it was preserved in the drilling mud. The drilling mud penetrate the sample through the pre-existing cracks. It increased very fast at first then stabilized. After it was taken out of the preserving fluids to get exposed, its weight started to decrease due to the exposure to air. The declining rate was very high at the start then slowed down. After around 684 hours, on April 27th, the fluctuation of the weight can be observed due to the loss or absorption of moisture content associated with the fluctuation of the relative humidity (the weight of sample J increased for some time then decreased).

It can be observed all the samples were losing weights after they were exposed to air. For the samples which were previously placed in a specific fluid, they showed weight gain due to the penetration of the preserving fluid (0.4% for sample A, 0.3% for sample H, 0.2% for sample J). Then they showed weight loss after they were left outside to get

exposed. The moisture loss included 2 stages. During the first stage the sample reaches pre-submersion weight and in the 2nd stage shown in the plot, its weight decreases below the initial weight shown in the plot. The moisture loss for sample B, D, E, F, G, and included only native moisture content. The moisture included two parts for sample A, H and J. and both losses happened at the same time:

1. Weight loss due to the loss of the preservation fluid (0.29 g for sample A, 0.18 g for sample H, 0.14 g for sample J).

2. Weight loss due to the loss of native moisture content (0.92 g for sample A, 0.73g for sample B, 7.47 g for sample D, 12.76 g for sample E, 0.58 g for sample F, 0.46 g for sample G, 0.50 g for sample H, 0.51 g for sample I, 0.26 g for sample J) .

The change of samples' weights was faster at the start of exposure then slowed down. The change of samples' weights fluctuated (the weights sometimes increased and sometimes decreased) due to the fluctuation of the relative humidity in the lab environment. This is related to the environment vapor pressure. The environment vapor pressure is in equilibrium with the capillary pressure between the shale layers. Once the environment vapor pressure was higher than the capillary pressure, the vapor would enter the  pre-existing cracks of shale. Therefore, the weight increased. As the environment relative humidity was sometimes higher and sometimes lower, the fluctuation of the weights for samples can be observed.

## 4.3 Acoustic velocity and dynamic mechanical properties' change over time

The error analysis for dynamic measurement is shown in Appendix.

Overall, these samples can be divided into three groups:

(1) The samples (B, D, E, F and G) that were brushed with a thin layer of decane after they were retrieved and stored in the cooler (Temperature in the cooler is 4℃). The 1-inch samples (B, F, G) were prepared by cutting large cores to chunks whose diameters were close to 1 inch, then the chunks were ground and polished to cylinders. The 4-inch samples' ends (D, E) were cut and polished (refer to Section 3.2 for details). The sample F was tested immediately after it was retrieved from the large core plugs. The exposure time during the preparation for sample B, D, E, F, and G were 272 mins, 116 mins, 138 mins, 115 mins, 146 mins. After each test, sample B, D, E, F, G were left outside to get exposed. They were tested every 24 hours initially. After some time, the exposure interval was increased to 48 hours, 96 hours gradually as the moisture loss tended to be less active.

(2) The samples (A, H) were retrieved from the large core plugs (like previous plugs). Sample H was then kept in the cooler by submerging it in the decane for preservation and later it was left in the open air after 144 hours. The exposure time during the preparation of sample H was 167 mins. Sample H served to investigate the impact of decane on the dynamic properties of organic-rich shale. A dynamic test was conducted every 24 hours while it was taken out of the decane and part-

42

dried (surface was dried). An axial load (3 MPa) was applied during each test to make sure good contact between the sample and platens. After each test, it was put back into the jar full of decane at the start. After 200 hours, sample H was left outside to get exposed and tested in the same manner as the samples in the first group.  After 552 hours, sample A was taken out of the KCl solution and kept in the open air. The exposure time during the preparation process is 296 mins for the sample A. Before testing, sample A was kept in the cooler for 552 hours while submerged in the KCl solution. Then sample A was taken out of the solutions and tested. An axial load (3 MPa for sample A) was applied during each test to make sure good contact between the sample and platens. After each test, it was left outside to get exposed without returning to the KCl solution.

(3) The samples (I, J) were retrieved from the same large core plugs (like previous plugs). The sample I and J were then kept in the cooler wrapped with plastic wrap for 22 hours and 18 hours respectively. The exposure time during the preparation of sample I and sample J was 131 mins, 123 mins respectively.

Sample I was tested in the way same as the samples in the group 1. Sample J served to investigate the impact of drilling mud on the dynamic properties of organic-rich shale. It was submerged in the 11.5 lb/gal drilling mud at the start. A dynamic test was conducted every 24 hours while it was taken out of the drilling mud and part-dried (surface was dried). An axial load (3 MPa) was applied during each test to make sure good contact between the sample and platens. After each test, it was put back into the jar full of drilling mud. After 456 hours, it was left

outside to get exposed and tested in the way for 392 hours same as samples in the group one.

## 4.3.1 Samples B, D, E, F, and G

Sample B, D, E, F, G were treated in a similar way i.e., preserved by brushing a thin layer of decane, wrapped with cling wrap then kept in the cooler (the only difference between them is the preservation time). During the preparation stage, their data were plotted together to study the impact of exposure to air on samples' elastic properties. As sample B, D, E and G were preserved by wrapping them with plastic wrap for the period before testing, sample F served to investigate whether the preservation time before testing would impact shale dynamic properties. Sample F was tested instantly after it became a plug then it is compared with the other samples in this group. The test results for sample B, D (in both vertical and horizontal direction), E, F, and G are shown in Table 15 to 19.

Table 16 Sample B dynamic test summary

| Date | Time (hour) | P-wave time (uS) | S-wave time (uS) | P velocity (m/s) | S velocity (m/s) | E (GPa) | v |
|------|------|------|------|------|------|------|------|
| 1/22 | 0 | 24.08 | 43.14 | 3954.73 | 2496.24 | 37.39 | 0.169 |
| 1/22 | 12 | 23.94 | 42.82 | 3987.99 | 2526.64 | 38.09 | 0.165 |
| 1/23 | 24 | 23.68 | 42.50 | 4051.25 | 2557.78 | 39.13 | 0.169 |
| 1/23 | 36 | 23.58 | 42.48 | 4076.12 | 2559.75 | 39.37 | 0.174 |
| 1/24 | 48 | 23.52 | 42.46 | 4091.19 | 2561.73 | 39.51 | 0.178 |
| 1/25 | 72 | 23.56 | 42.46 | 4081.13 | 2561.73 | 39.39 | 0.175 |
| 1/26 | 96 | 23.48 | 42.44 | 4101.30 | 2563.71 | 39.59 | 0.179 |
| 1/27 | 120 | 23.38 | 42.50 | 4126.17 | 2557.40 | 39.68 | 0.188 |
| 1/29 | 168 | 23.30 | 42.38 | 4146.78 | 2569.27 | 40.01 | 0.188 |
| 1/31 | 216 | 23.26 | 42.32 | 4157.17 | 2575.25 | 40.20 | 0.189 |
| 2/2 | 264 | 23.16 | 41.94 | 4183.36 | 2613.78 | 41.08 | 0.180 |
| 2/5 | 336 | 26.42 | 44.04 | 3470.47 | 2414.18 | 30.62 | 0.031 |
| 2/7 | 384 | 25.83 | 43.94 | 3580.91 | 2422.99 | 32.22 | 0.078 |
| 2/9 | 432 | 25.67 | 43.78 | 3612.08 | 2437.22 | 32.73 | 0.082 |
| 2/11 | 480 | 25.65 | 43.76 | 3616.01 | 2439.02 | 32.79 | 0.083 |
| 2/16 | 600 | 26.05 | 43.76 | 3538.91 | 2439.02 | 31.75 | 0.048 |
| 2/22 | 744 | 25.89 | 43.28 | 3569.35 | 2482.80 | 32.38 | 0.031 |
| 2/28 | 888 | 25.97 | 43.44 | 3554.07 | 2468.03 | 32.11 | 0.034 |
| 3/3 | 960 | 25.81 | 43.36 | 3584.77 | 2475.39 | 32.60 | 0.044 |
| 3/9 | 1104 | 25.74 | 43.28 | 3598.37 | 2482.80 | 32.82 | 0.046 |

Table 17 Sample D dynamic test summary in the vertical direction

| Date | Time (hour) | P-wave time (uS) | S-wave time (uS) | P velocity (m/s) | S velocity (m/s) | E (GPa) | v |
|------|------|------|------|------|------|------|------|
| 1/22 | 0 | 21.58 | 36.74 | 3768.49 | 2168.75 | 29.92 | 0.252 |
| 1/22 | 12 | 21.29 | 36.70 | 3839.46 | 2171.93 | 30.31 | 0.265 |
| 1/23 | 24 | 21.15 | 36.66 | 3874.69 | 2175.13 | 30.52 | 0.270 |
| 1/23 | 36 | 21.05 | 36.34 | 3900.25 | 2201.04 | 31.04 | 0.266 |
| 1/24 | 48 | 20.97 | 36.28 | 3920.94 | 2205.97 | 31.23 | 0.268 |
| 1/25 | 72 | 20.91 | 36.26 | 3936.61 | 2207.62 | 31.33 | 0.271 |
| 1/26 | 96 | 20.87 | 35.98 | 3947.12 | 2230.94 | 31.87 | 0.265 |
| 1/27 | 120 | 20.81 | 35.54 | 3963.00 | 2268.61 | 32.72 | 0.256 |
| 1/29 | 168 | 20.78 | 34.10 | 3970.98 | 2401.30 | 35.36 | 0.212 |
| 1/31 | 216 | 20.70 | 34.04 | 3992.44 | 2407.17 | 35.60 | 0.214 |
| 2/2 | 264 | 20.70 | 32.74 | 3992.44 | 2541.70 | 37.87 | 0.159 |
| 2/5 | 336 | 20.72 | 33.76 | 3987.05 | 2434.93 | 36.04 | 0.203 |
| 2/7 | 408 | 20.71 | 34.82 | 3989.74 | 2333.07 | 34.12 | 0.240 |
| 2/9 | 456 | 20.81 | 34.18 | 3963.00 | 2393.52 | 35.11 | 0.213 |
| 2/11 | 504 | 20.83 | 34.16 | 3957.69 | 2395.46 | 35.10 | 0.211 |
| 2/16 | 624 | 20.82 | 34.16 | 3960.34 | 2395.46 | 35.12 | 0.212 |
| 2/22 | 768 | 20.77 | 33.28 | 3973.65 | 2484.03 | 36.74 | 0.179 |
| 2/28 | 912 | 20.85 | 33.36 | 3952.40 | 2475.71 | 36.43 | 0.177 |
| 3/3 | 984 | 20.82 | 33.28 | 3960.34 | 2484.03 | 36.62 | 0.176 |
| 3/9 | 1128 | 20.80 | 33.28 | 3965.66 | 2484.03 | 36.65 | 0.177 |

Table 18 Sample D dynamic test summary in the horizontal direction

| Date | Time (hour) | P-ave time (uS) | S-wave time (uS) | P velocity (m/s) | S velocity (m/s) | E (Pa) | v |
|------|-------------|-----------------|------------------|------------------|------------------|--------|---|
| 1/22 | 0 | 22.60 | 36.90 | 4428.32 | 2712.20 | 44.84 | 0.200 |
| 1/22 | 12 | 22.57 | 36.82 | 4434.20 | 2718.09 | 45.00 | 0.199 |
| 1/23 | 24 | 22.53 | 42.82 | 4442.08 | 2725.49 | 45.21 | 0.198 |
| 1/23 | 36 | 22.45 | 42.66 | 4457.91 | 2737.42 | 45.40 | 0.197 |
| 1/24 | 48 | 22.42 | 42.54 | 4463.87 | 2746.43 | 45.63 | 0.195 |
| 1/25 | 72 | 22.40 | 42.38 | 4467.86 | 2758.54 | 45.90 | 0.192 |
| 1/26 | 96 | 22.42 | 42.22 | 4463.87 | 2770.76 | 46.10 | 0.187 |
| 1/27 | 120 | 22.37 | 42.02 | 4473.85 | 2786.19 | 46.48 | 0.183 |
| 1/29 | 168 | 22.41 | 41.62 | 4465.86 | 2817.57 | 46.98 | 0.169 |
| 1/31 | 216 | 22.46 | 41.50 | 4455.92 | 2827.12 | 47.03 | 0.163 |
| 2/2 | 264 | 22.66 | 41.32 | 4416.59 | 2841.57 | 46.83 | 0.147 |
| 2/5 | 336 | 22.50 | 40.92 | 4448.00 | 2874.21 | 47.67 | 0.142 |

Table 19 Sample E dynamic test summary

| Date | Time (hour) | P-wave time (uS) | S-wave time (uS) | P velocity (m/s) | S velocity (m/s) | E (GPa) | v |
|------|-------------|------------------|------------------|------------------|------------------|---------|---|
| 2-Jan | 0 | 32.84 | 57.10 | 3818.09 | 2160.65 | 29.29 | 0.264 |
| 2-Jan | 12 | 32.84 | 57.08 | 3818.09 | 2161.55 | 29.29 | 0.264 |
| 3-Jan | 24 | 32.84 | 57.04 | 3818.09 | 2163.37 | 29.31 | 0.264 |
| 4-Jan | 48 | 32.88 | 57.02 | 3812.44 | 2164.28 | 29.29 | 0.262 |
| 4-Jan | 60 | 32.92 | 56.96 | 3806.79 | 2167.02 | 29.32 | 0.260 |
| 5-Jan | 72 | 32.96 | 57.00 | 3801.17 | 2165.19 | 29.24 | 0.260 |
| 6-Jan | 96 | 32.96 | 57.04 | 3801.17 | 2163.37 | 29.21 | 0.260 |
| 7-Jan | 120 | 33.04 | 56.88 | 3789.97 | 2170.68 | 29.30 | 0.256 |
| 8-Jan | 144 | 32.98 | 56.72 | 3798.36 | 2178.03 | 29.46 | 0.255 |
| 9-Jan | 168 | 32.84 | 56.64 | 3818.09 | 2181.72 | 29.62 | 0.258 |
| 12-Jan | 240 | 32.64 | 56.52 | 3846.64 | 2187.29 | 29.84 | 0.261 |
| 14-Jan | 288 | 32.60 | 56.46 | 3852.40 | 2190.08 | 29.92 | 0.261 |
| 17-Jan | 360 | 32.72 | 56.48 | 3835.17 | 2189.15 | 29.80 | 0.258 |
| 20-Jan | 432 | 32.68 | 56.60 | 3840.90 | 2183.57 | 29.71 | 0.261 |
| 22-Jan | 480 | 32.72 | 56.52 | 3835.17 | 2187.29 | 29.76 | 0.259 |
| 24-Jan | 528 | 32.80 | 56.24 | 3823.77 | 2200.38 | 29.95 | 0.252 |
| 27-Jan | 600 | 32.76 | 56.68 | 3829.46 | 2179.87 | 29.57 | 0.260 |
| 31-Jan | 696 | 33.22 | 53.36 | 3765.00 | 2344.80 | 32.11 | 0.183 |
| 3-Feb | 768 | 33.38 | 52.76 | 3743.09 | 2377.31 | 32.41 | 0.162 |
| 7-Feb | 840 | 33.35 | 53.16 | 3747.18 | 2355.54 | 32.12 | 0.173 |
| 11-Feb | 936 | 33.33 | 52.56 | 3749.91 | 2388.35 | 32.60 | 0.159 |
| 16-Feb | 1056 | 33.28 | 52.45 | 3756.75 | 2394.46 | 32.75 | 0.158 |
| 22-Feb | 1200 | 33.26 | 52.41 | 3759.50 | 2396.69 | 32.79 | 0.158 |
| 28-Feb | 1344 | 33.49 | 52.92 | 3728.17 | 2368.55 | 32.14 | 0.162 |
| 3-Mar | 1416 | 33.41 | 52.88 | 3739.01 | 2370.74 | 32.25 | 0.164 |
| 9-Mar | 1560 | 33.33 | 52.81 | 3749.91 | 2374.57 | 32.39 | 0.165 |

Table 20 Sample F dynamic test summary

| Date | Time (hour) | P-wave time (uS) | S-wave time (uS) | P velocity (m/s) | S velocity (m/s) | E (GPa) | v |
|------|------|------|------|------|------|------|------|
| 1/30 | 0 | 21.02 | 38.38 | 3801.89 | 2390.11 | 34.14 | 0.173 |
| 1/31 | 16 | 20.94 | 38.22 | 3824.18 | 2407.75 | 34.50 | 0.172 |
| 1/31 | 24 | 20.84 | 37.82 | 3852.40 | 2453.01 | 35.40 | 0.159 |
| 2/1 | 40 | 20.76 | 37.58 | 3875.28 | 2480.99 | 35.98 | 0.153 |
| 2/1 | 48 | 20.74 | 37.50 | 3881.04 | 2490.46 | 36.16 | 0.150 |
| 2/2 | 64 | 20.68 | 37.46 | 3898.43 | 2495.22 | 36.36 | 0.153 |
| 2/2 | 73 | 20.64 | 37.40 | 3910.11 | 2502.40 | 36.57 | 0.153 |
| 2/3 | 90 | 20.62 | 37.42 | 3915.98 | 2500.00 | 36.57 | 0.156 |
| 2/3 | 100 | 20.60 | 37.42 | 3921.86 | 2500.00 | 36.62 | 0.158 |
| 2/4 | 120 | 20.56 | 37.34 | 3933.69 | 2509.62 | 36.86 | 0.157 |
| 2/5 | 139 | 20.97 | 37.88 | 3815.79 | 2446.11 | 34.83 | 0.151 |
| 2/6 | 161 | 20.95 | 37.94 | 3821.38 | 2439.25 | 34.78 | 0.156 |
| 2/7 | 191 | 20.71 | 37.62 | 3889.72 | 2476.28 | 35.92 | 0.159 |
| 2/8 | 215 | 20.71 | 37.62 | 3889.72 | 2476.28 | 35.92 | 0.159 |
| 2/9 | 234 | 20.71 | 37.62 | 3889.72 | 2476.28 | 35.91 | 0.159 |
| 2/10 | 258 | 20.67 | 37.54 | 3901.35 | 2485.71 | 36.15 | 0.158 |
| 2/11 | 282 | 20.67 | 37.54 | 3901.35 | 2485.71 | 36.15 | 0.158 |
| 2/12 | 306 | 20.67 | 37.46 | 3901.35 | 2495.22 | 36.28 | 0.154 |
| 2/14 | 354 | 20.66 | 37.44 | 3904.26 | 2497.61 | 36.34 | 0.154 |
| 2/16 | 402 | 20.94 | 37.36 | 3824.18 | 2507.20 | 35.67 | 0.123 |
| 2/19 | 474 | 20.94 | 37.46 | 3824.18 | 2495.22 | 35.53 | 0.129 |
| 2/22 | 546 | 20.86 | 37.33 | 3846.72 | 2510.82 | 35.94 | 0.129 |
| 2/25 | 618 | 20.78 | 37.28 | 3869.53 | 2516.88 | 36.25 | 0.133 |
| 2/28 | 690 | 20.82 | 37.36 | 3858.09 | 2507.20 | 36.03 | 0.134 |
| 3/3 | 762 | 20.78 | 37.33 | 3869.53 | 2510.82 | 36.18 | 0.136 |
| 3/9 | 906 | 20.74 | 37.29 | 3881.04 | 2515.66 | 36.35 | 0.138 |

Table 21 Sample G dynamic test summary

| Date | Time (hour) | P-wave time (uS) | S-wave time (uS) | P velocity (m/s) | S velocity (m/s) | E (GPa) | v |
|------|------|------|------|------|------|------|------|
| 2/1 | 0 | 15.80 | 32.22 | 4459.46 | 2420.28 | 39.15 | 0.291 |
| 2/2 | 16 | 15.78 | 32.20 | 4469.96 | 2423.37 | 39.14 | 0.292 |
| 2/2 | 25 | 15.76 | 32.18 | 4480.52 | 2426.47 | 39.23 | 0.292 |
| 2/3 | 42 | 15.75 | 31.34 | 4485.82 | 2564.19 | 42.59 | 0.257 |
| 2/3 | 52 | 15.75 | 31.92 | 4485.82 | 2467.49 | 40.23 | 0.283 |
| 2/4 | 71 | 15.75 | 31.66 | 4485.82 | 2509.92 | 41.25 | 0.272 |
| 2/5 | 89 | 15.73 | 32.10 | 4496.45 | 2438.95 | 39.51 | 0.292 |
| 2/6 | 112 | 15.71 | 32.34 | 4507.13 | 2401.90 | 38.60 | 0.302 |
| 2/7 | 142 | 15.75 | 32.31 | 4485.82 | 2406.47 | 38.62 | 0.298 |
| 2/8 | 166 | 15.75 | 32.28 | 4485.82 | 2411.05 | 38.72 | 0.297 |
| 2/9 | 185 | 15.75 | 32.15 | 4485.82 | 2431.13 | 39.22 | 0.292 |
| 2/10 | 209 | 15.67 | 31.96 | 4528.64 | 2461.09 | 40.13 | 0.290 |
| 2/11 | 233 | 15.65 | 31.86 | 4539.47 | 2477.15 | 40.58 | 0.288 |
| 2/12 | 257 | 15.65 | 31.83 | 4539.47 | 2482.01 | 40.68 | 0.287 |
| 2/14 | 305 | 15.71 | 31.86 | 4507.13 | 2477.15 | 40.42 | 0.284 |
| 2/16 | 353 | 16.34 | 32.37 | 4193.37 | 2397.35 | 37.09 | 0.257 |
| 2/19 | 425 | 16.36 | 32.37 | 4184.12 | 2397.35 | 37.05 | 0.256 |
| 2/22 | 497 | 16.34 | 32.48 | 4193.37 | 2380.80 | 36.71 | 0.262 |
| 2/25 | 569 | 16.32 | 32.42 | 4202.66 | 2389.80 | 36.95 | 0.261 |
| 2/28 | 641 | 16.42 | 32.56 | 4156.63 | 2368.91 | 36.28 | 0.259 |
| 3/3 | 713 | 16.30 | 32.37 | 4211.99 | 2397.35 | 37.17 | 0.260 |
| 3/9 | 857 | 16.22 | 32.29 | 4249.72 | 2409.52 | 37.61 | 0.263 |

Figure 22 shows the change of P-wave velocity over time for sample B, D (both in the horizontal and vertical direction), E, F, G.
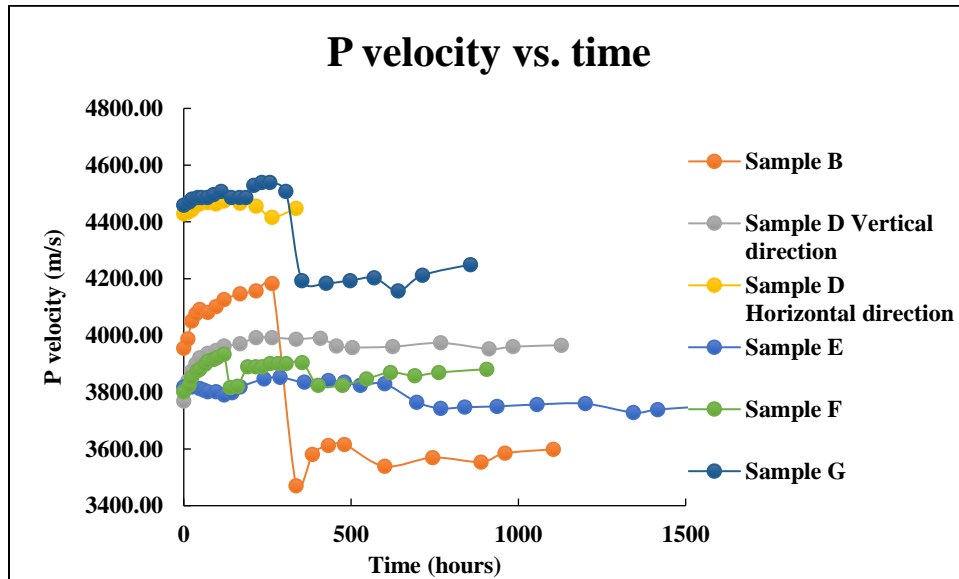


Figure 22 Change of P velocity over time for sample B, D (vertical and horizontal direction), E, F, G

The P-wave velocity increased slightly during the early time exposure for samples B, D (in both vertical direction and horizontal direction), and for samples F, G (due to the contraction of shale samples caused by the capillary confining effect). The P-wave velocity of the sample B suddenly decreased at around 336 hours. P-wave velocity of sample F, G also suddenly decreased at around 139 hours and 353 hours (due to the formation of fractures), respectively. After the sudden drop of P-wave velocity of sample B, F, G, their P-wave velocity still show an increasing trend (as the continuous moisture loss still act as a confining effect (shrinkage)). The measurement in the horizontal direction for sample D was stopped at around 400 hours due to the loss of the signal in the horizontal direction (as dynamic signal would be attenuated with the growth of cracks).

48

The P -wave velocity didn't show obvious change at the start for sample E. Sample E was with the least cracks shown in the CT image. Therefore, it took a longer time for moisture loss to show impact on sample E's P-wave velocity. Then at 696 hours, it decreased.

Figure 23 shows the S velocity change over time for sample B, D (both in the horizontal and vertical direction), E, F, G.
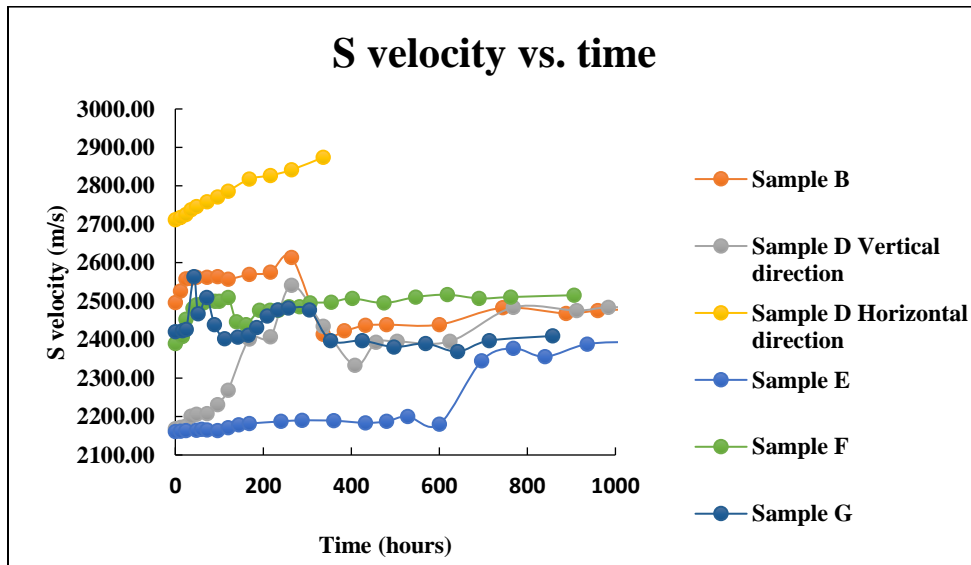


Figure 23 Change of S velocity over time for sample B, D, E, F, G

The S-wave velocity increased slightly for sample B, D (in both vertical and horizontal directions), F, G at the start of exposure (due to the contraction of shale samples). The S-wave velocity of B suddenly decreased at around 336 hours. The S-wave velocity of sample D, F, G decreased at 336 hours, 139 hours, 353 hours respectively. The decrease was due to the formation of fractures. The measurement in the horizontal direction of sample D was stopped at around 400 hours due to the loss of the signal (as dynamic signal

49

was attenuated with the growth of cracks). The change of S-wave velocity of sample E is not obvious at the start. Sample E is a big 4-inch sample with the least cracks shown in the CT image. Therefore, it took a longer time for the moisture loss to show impact on its S-wave velocity. Then at 696 hours, it suddenly increased.

Figure 24 shows the Poisson's ratio change over time for sample B, D (in both horizontal and vertical directions), E, F, G.
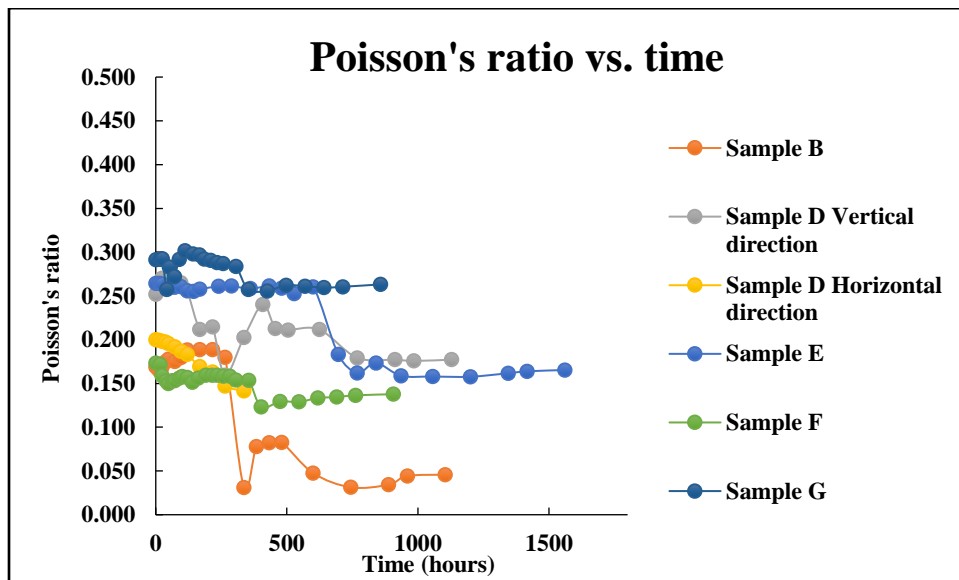


Figure 24 Change of Poisson's ratio over time for sample B, D, E, F, G

Poisson's ratio stayed stable for sample B, D, E, F, G over time at the start of exposure as P-wave velocity and S-wave velocity increased at a similar rate (Poisson's ratio was calculated by using the ratio between S-wave velocity and P-wave velocity). Poisson's ratio of B suddenly decreased at around 336 hours (due to the formation of fractures). Poisson's ratio of sample D, E, F, G also decreased at 336hours, 696 hours, 139 hours, 353 hours (because of the fractures formed). The measurement in the horizontal direction

for sample D is stopped at around 400 hours due to the loss of the signal (as dynamic signal would be attenuated with the growth of cracks).

Figure 25 shows the change of Young's modulus over time for sample B, D (both in the horizontal and vertical direction), E, F, G.
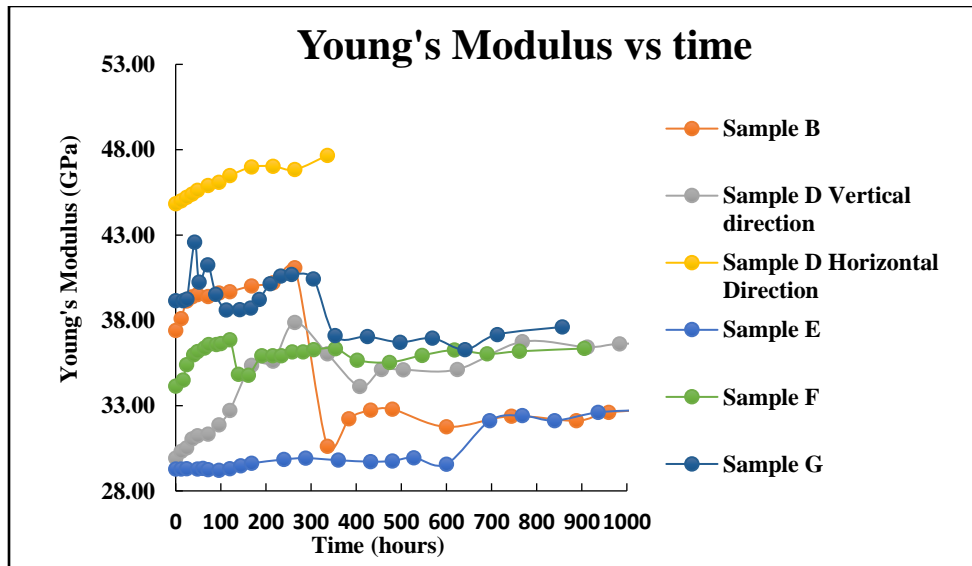


Figure 25 Change of Young's modulus over time for sample B, D, E, F, G

Young's modulus increased for sample B, D, F, G (due to the capillary confining effect caused buy the loss of moisture content at the start of exposure. This confining effect will make shale contract). Young's modulus of B suddenly decreased at around 336 hours. Young's modulus of sample D, F, G also decreased at 336 hours, 139 hours, 353 hours respectively. These decreases were due to the formation of fractures under excessive exposure. The measurement in the horizontal direction for sample D is stopped at around 400 hours due to the loss of the signal (as dynamic was attenuated with the growth of

cracks). Young's modulus for sample E suddenly increased at around 696 hours (due to the contraction of shale sample and capillary confining effect).

Young's modulus and Poisson's ratio change percentage over time for sample B, D, E, F, G can be shown in Figure 26 and Figure 27. The percentage value is calculated relative to the data measured by the first test. Note that the elastic properties are calculated assuming that the theory is still valid for these shales as their saturation changes, and this may not be the case.
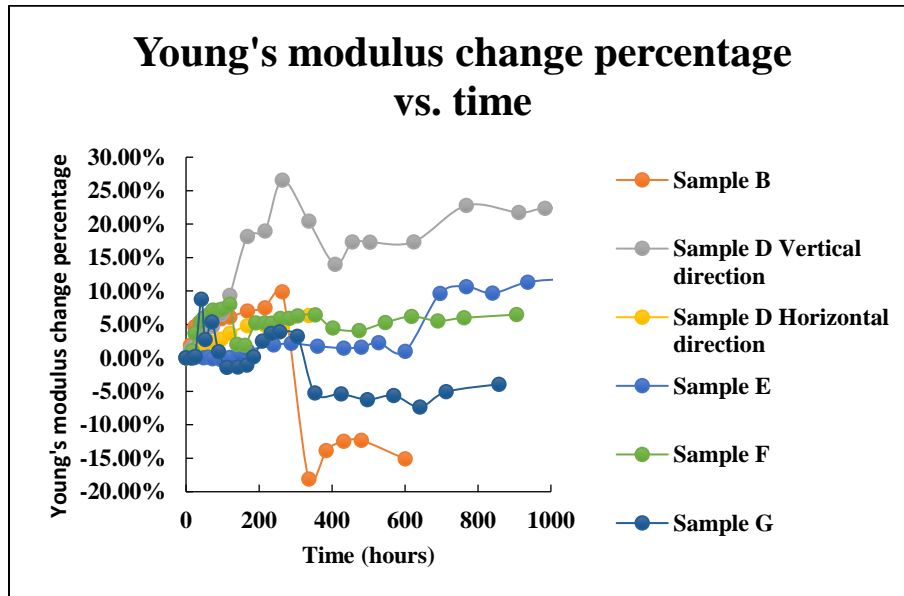


Figure 26 Change of Young's Modulus in percentage over time for sample B, D, F, G
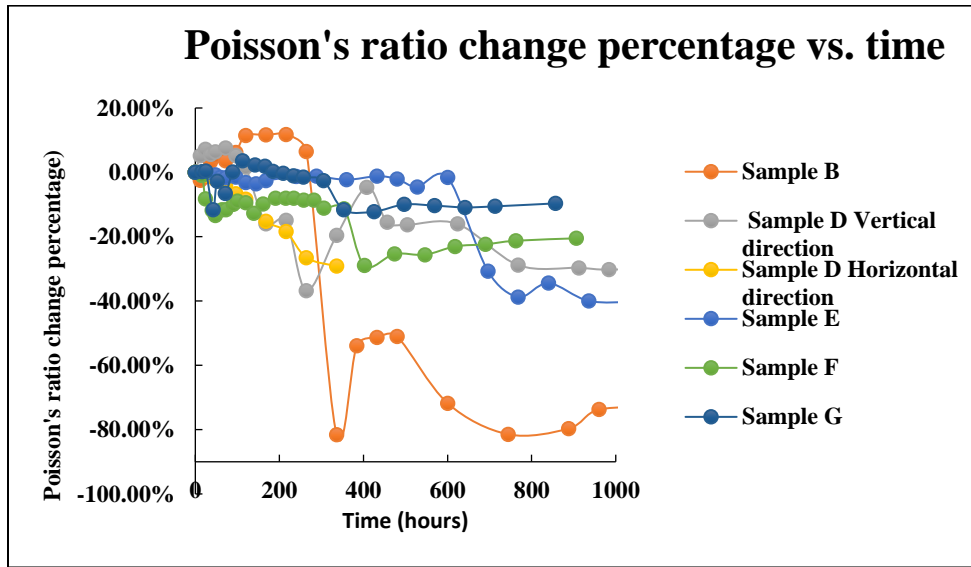
Figure 27 Change of Poisson's ratio in percentage over time for sample B, D, F, G

## 4.3.2 Samples A and H

As sample A and H are treated in a similar way except having used different preservation

fluid types during the preparation process.:

1. Sample A was preserved in the 7% KCl solution

2. Sample H was preserved in the decane.

They are plotted together to study the impact of the different types of preservation fluids

on the shale elastic properties. The test was also conducted while sample H was still under

preservation. We treated the time when sample H was taken out of the preservation fluid

as time 0. It was assumed the fluids only have physical impact on shale samples in this

case. The chemical reaction between the fluids and shale samples were not considered in

this case. The dynamic test summary for sample A and sample H are shown in Table 21 and Table 22.

Table 22 Dynamic test summary for sample A

| Date | Time (hour) | P-wave time (uS) | S-wave time (uS) | P velocity (m/s) | S velocity (m/s) | E (GPa) | v |
|---|---|---|---|---|---|---|---|
| 1/22 | 0 | 24.78 | 46.34 | 4051.46 | 2377.85 | 36.04 | 0.237 |
| 1/22 | 12 | 25.04 | 45.78 | 3992.11 | 2423.39 | 36.38 | 0.208 |
| 1/23 | 24 | 25.94 | 45.72 | 3799.46 | 2428.38 | 34.85 | 0.155 |
| 1/23 | 36 | 26.10 | 45.62 | 3767.15 | 2436.73 | 34.61 | 0.140 |
| 1/24 | 48 | 26.34 | 45.46 | 3719.69 | 2450.21 | 34.24 | 0.117 |
| 1/25 | 72 | 26.48 | 45.44 | 3692.55 | 2451.90 | 33.93 | 0.106 |
| 1/26 | 96 | 26.50 | 45.40 | 3686.62 | 2453.92 | 33.87 | 0.102 |
| 1/27 | 120 | 26.64 | 45.38 | 3658.91 | 2454.92 | 33.53 | 0.091 |
| 1/29 | 168 | 26.58 | 45.30 | 3670.30 | 2461.75 | 33.70 | 0.091 |
| 1/31 | 216 | 26.54 | 45.30 | 3677.92 | 2461.75 | 33.78 | 0.094 |
| 2/2 | 264 | 26.66 | 44.90 | 3655.14 | 2496.47 | 33.72 | 0.063 |
| 2/5 | 336 | 26.68 | 45.16 | 3651.37 | 2473.79 | 33.51 | 0.076 |
| 2/7 | 384 | 26.63 | 45.78 | 3660.81 | 2421.34 | 33.15 | 0.111 |
| 2/9 | 432 | 26.68 | 45.70 | 3651.37 | 2427.98 | 33.10 | 0.104 |
| 2/11 | 480 | 26.65 | 45.68 | 3657.02 | 2429.65 | 33.18 | 0.105 |
| 2/16 | 600 | 27.52 | 46.61 | 3499.75 | 2354.51 | 30.67 | 0.087 |
| 2/22 | 744 | 27.17 | 46.48 | 3561.37 | 2364.73 | 31.47 | 0.106 |
| 2/28 | 888 | 27.25 | 46.64 | 3547.09 | 2352.16 | 31.21 | 0.108 |
| 3/3 | 960 | 27.41 | 46.28 | 3518.89 | 2380.63 | 31.10 | 0.078 |
| 3/9 | 1104 | 27.33 | 45.92 | 3532.93 | 2409.80 | 31.47 | 0.065 |

Table 23 Dynamic test summary for sample H

| Date | Time (hour) | P-wave time (uS) | S-wave time (uS) | P velocity (m/s) | S velocity (m/s) | E (GPa) | v |
|---|---|---|---|---|---|---|---|
| 2/2 | -144 | 18.90 | 35.22 | 3882.00 | 2412.74 | 34.99 | 0.185 |
| 2/3 | -120 | 18.24 | 35.42 | 4115.98 | 2387.18 | 36.10 | 0.247 |
| 2/4 | -96 | 17.92 | 35.50 | 4239.89 | 2377.11 | 36.50 | 0.271 |
| 2/5 | -72 | 17.87 | 35.59 | 4259.92 | 2365.88 | 36.34 | 0.277 |
| 2/6 | -53 | 17.87 | 35.63 | 4259.92 | 2360.92 | 36.24 | 0.278 |
| 2/8 | 0 | 17.87 | 35.59 | 4259.92 | 2365.88 | 36.36 | 0.277 |
| 2/9 | 18 | 18.91 | 35.62 | 3875.22 | 2360.06 | 31.52 | 0.205 |
| 2/9 | 29 | 19.27 | 35.62 | 3758.76 | 2360.06 | 30.68 | 0.175 |
| 2/10 | 43 | 19.35 | 35.54 | 3733.83 | 2370.00 | 30.60 | 0.163 |
| 2/11 | 66 | 19.48 | 35.51 | 3694.01 | 2373.75 | 30.28 | 0.148 |
| 2/12 | 90 | 19.69 | 35.51 | 3631.45 | 2373.75 | 29.68 | 0.127 |
| 2/13 | 115 | 19.71 | 35.49 | 3625.60 | 2376.25 | 29.64 | 0.123 |
| 2/14 | 139 | 19.70 | 35.50 | 3628.53 | 2375.00 | 29.65 | 0.125 |
| 2/15 | 163 | 19.68 | 35.44 | 3634.38 | 2382.54 | 29.79 | 0.123 |
| 2/16 | 187 | 19.66 | 35.42 | 3640.26 | 2385.06 | 29.86 | 0.124 |
| 2/19 | 259 | 19.72 | 35.44 | 3622.69 | 2382.54 | 29.66 | 0.119 |
| 2/22 | 331 | 19.70 | 35.40 | 3628.53 | 2387.59 | 29.74 | 0.118 |
| 2/25 | 403 | 20.58 | 36.48 | 3388.26 | 2258.27 | 26.17 | 0.100 |
| 2/28 | 475 | 19.86 | 35.76 | 3582.34 | 2342.87 | 28.84 | 0.126 |
| 3/3 | 547 | 20.46 | 36.26 | 3419.13 | 2283.47 | 26.68 | 0.097 |
| 3/9 | 691 | 20.14 | 36.13 | 3504.28 | 2298.62 | 27.63 | 0.122 |

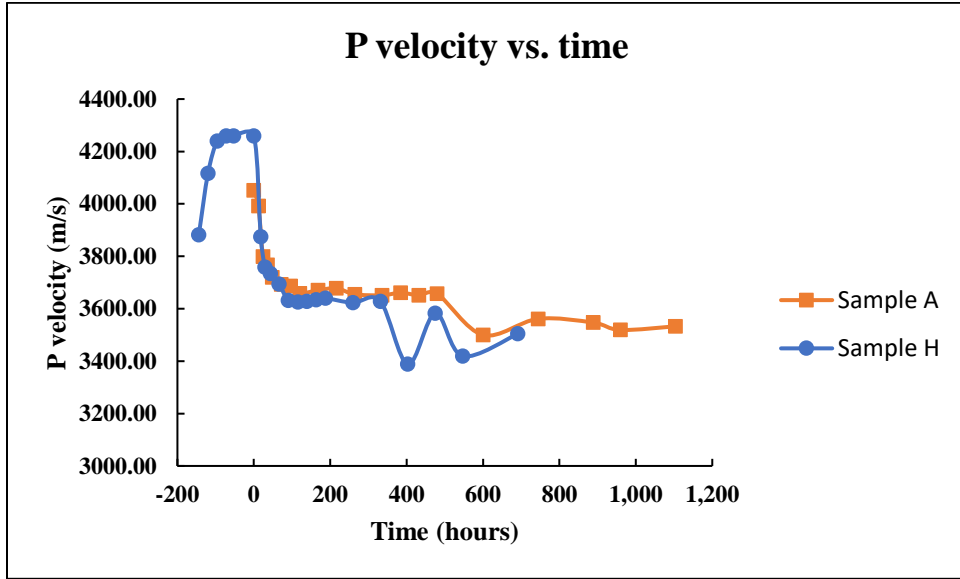Figure 28 shows the P velocity change over time for sample A and H.



Figure 28 Change of P velocity over time for sample A and H

P-wave velocity for sample H increased under preservation (due to the penetration of decane through the pre-existing cracks). Sample A and sample H showed a very similar behavior after they were taken out of the preservation fluid. When sample A and H were taken out of the preservation condition and exposed to air, their P-wave velocities decreased at first and then stabilized (due to the loss of the preserving fluid which has penetrated through the cracks while under preservation). A sudden drop of P-wave velocity was observed for both samples after exposing 600 hours and 403 hours for sample A and sample H respectively (due to the formation of fractures)

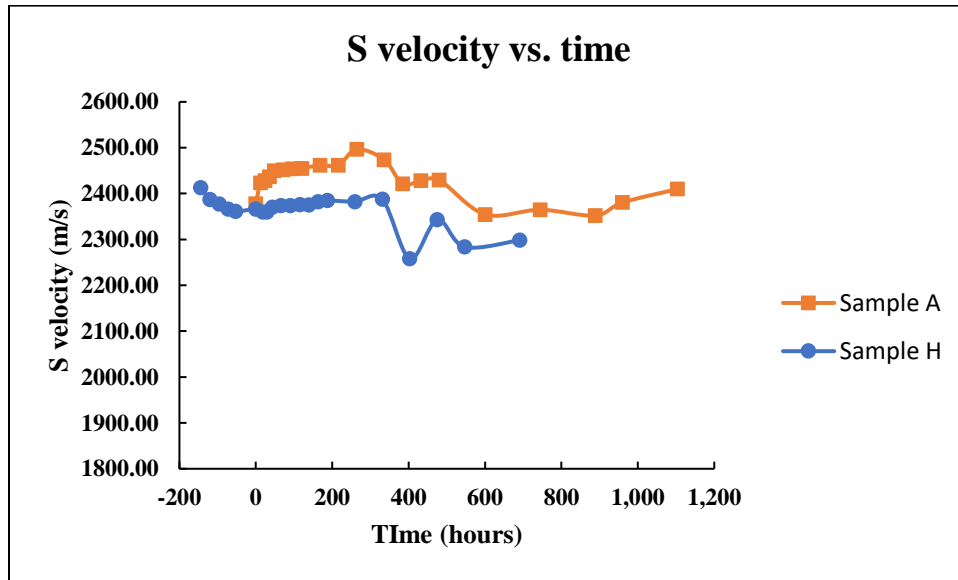Figure 29 shows the change in S velocity for sample A and H over time.

Figure 29 Change of S velocity over time for sample A and H

S-wave velocity for sample H remained stable while in the fluid (as the penetration of decane (fluid) won't impact on S-wave velocity). Then, when sample A and H were taken out of the preservation conditions, their S-wave velocities remained stable because the loss of preserving fluid does not affect the S-wave velocity. A sudden drop of S-wave velocity was observed after exposing 600 hours and 403 hours for sample A and sample H respectively due to the formation of fractures

Figure 25 shows the change of the Poisson's ratio for sample A and H over time.
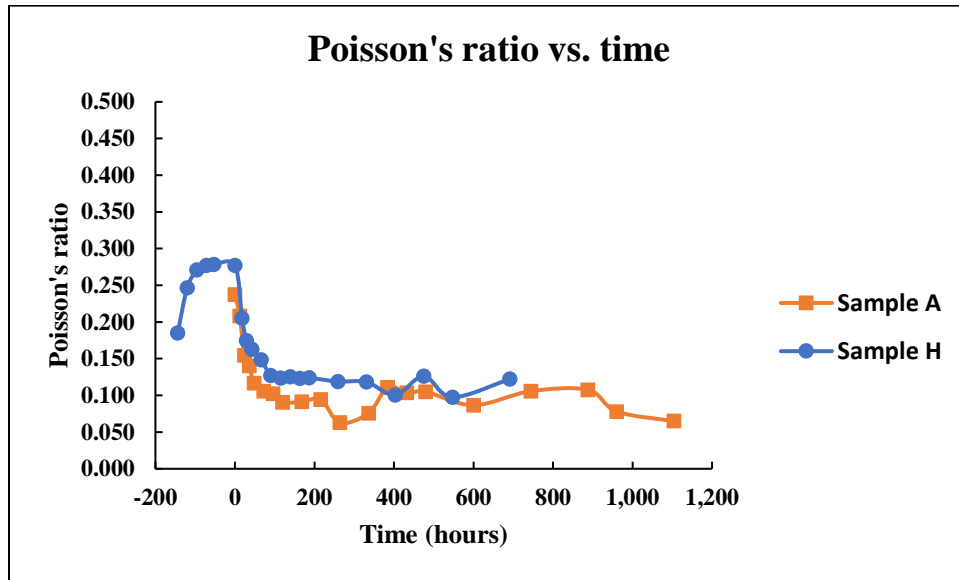
Figure 30 Change of Poisson's ratio over time for sample A and H

Poisson's ratio for sample H increased then stayed stable while under preservation due to the penetration of decane through the pre-existing cracks. When sample A and H were taken out of the preservation, their Poisson's ratio began to decrease because of the loss of preserving fluid. A sudden drop of Poisson's ratio was observed after exposing 600 hours and 403 hours for sample A and sample H respectively because of the formed fractures.

Figure 26 shows the change of Young's modulus over time for sample A and H.
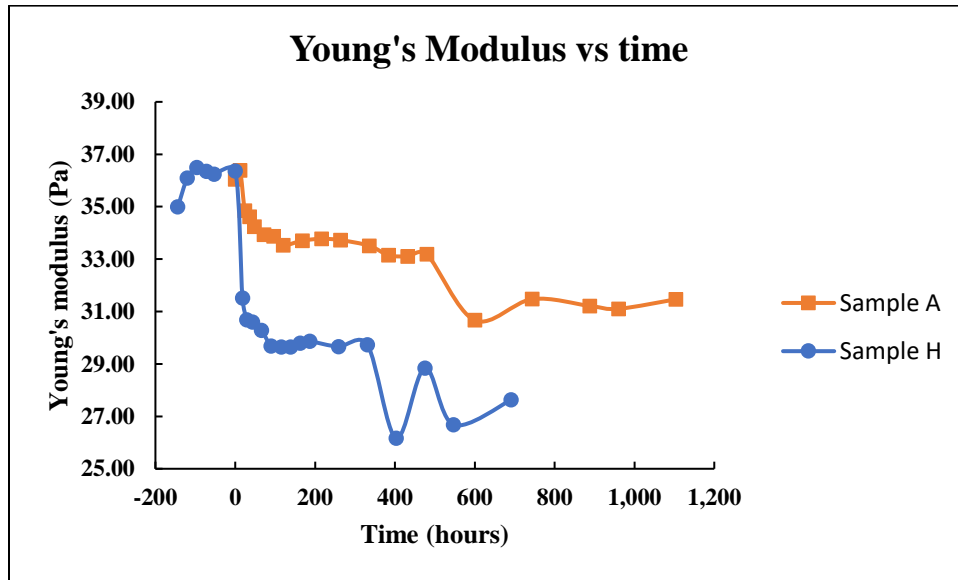
Figure 31 Change of Young's modulus over time for sample A and H

The Young's modulus increased then stabilized for sample H while under preservation due to the penetration of decane through the pre-existing cracks. Then when sample A and sample H were taken out of the fluids to get exposed, their Young's modulus began to decrease due to the loss of the preserving fluid. A sudden drop of Young's modulus was observed after exposing 600 hours and 403 hours for sample A and sample H respectively due to the formation of the fractures.

Therefore, Young's modulus and Poisson's ratio change percentage over time for sample A and H can be shown in Figure 32 and Figure 33. The percentage value is calculated relative to the data measured by the first test. Note that the elastic properties are calculated assuming that the theory is still valid for these shales as their saturation changes, and this may not be the case.
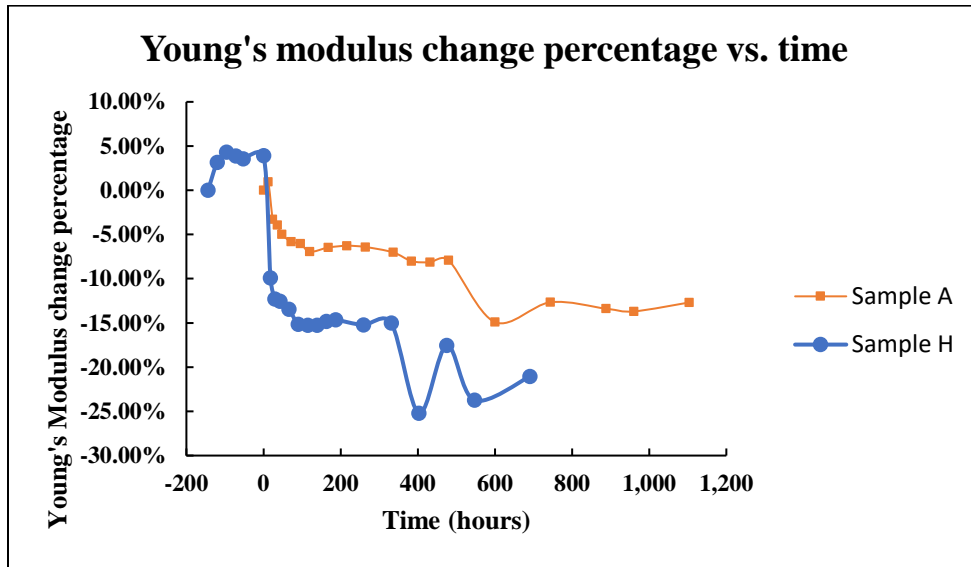
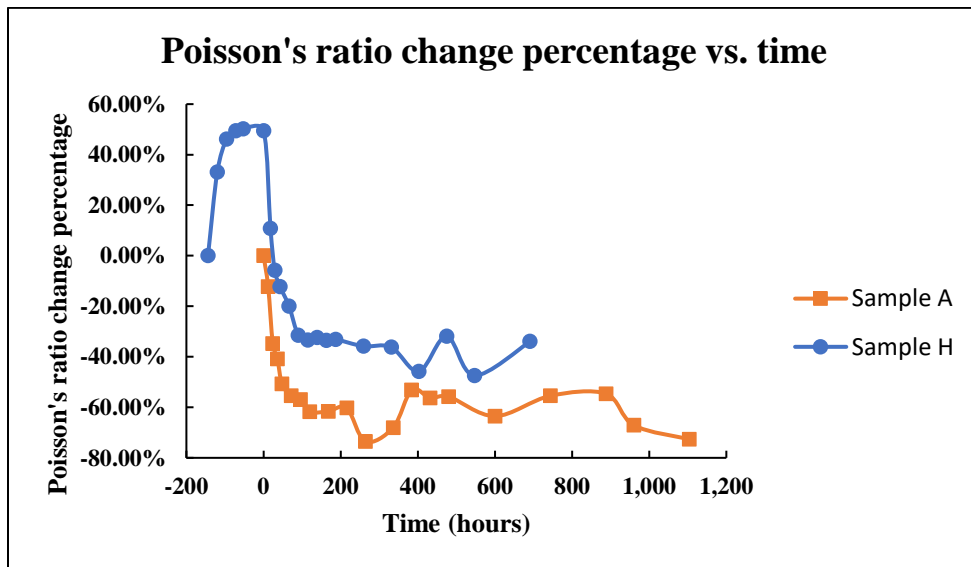Figure 32 Change of Young's Modulus in percentage over time for sample A and C



Figure 33 Change of Poisson's ratio in percentage over time for sample A and C

### 4.3.3 Samples I and J

Sample I and sample J were cored from the same interval. Sample I and J were preserved by wrapping with cling wrap then placed in the cooler for 20 hours before being tested. After the first test (sample I and sample J was tested exactly at the same time), sample I was left to the open air to be exposed. Sample J was put into a jar full of 11.5 lb/gal NaCl-based drilling mud. It was taken out of the drilling mud to get exposed after its weight stabilized at about 456 hours.

Table 24 Dynamic test summary for sample I

| Date | Time (hour) | P-wave time (uS) | S-wave time (uS) | P velocity (m/s) | S velocity (m/s) | E (GPa) | v |
|------|-------------|------------------|------------------|------------------|------------------|---------|---|
| 3/30 | 0 | 22.05 | 40.48 | 3798.78 | 2342.11 | 33.22 | 0.193 |
| 3/30 | 12 | 21.97 | 40.24 | 3819.48 | 2365.82 | 33.69 | 0.189 |
| 3/31 | 24 | 21.73 | 39.84 | 3882.96 | 2406.44 | 34.80 | 0.188 |
| 3/31 | 36 | 21.65 | 39.76 | 3904.60 | 2414.73 | 35.10 | 0.190 |
| 4/1 | 48 | 21.57 | 39.68 | 3926.47 | 2423.08 | 35.38 | 0.192 |
| 4/1 | 60 | 21.53 | 39.64 | 3937.50 | 2427.27 | 35.51 | 0.194 |
| 4/2 | 72 | 21.57 | 39.60 | 3926.47 | 2431.48 | 35.48 | 0.189 |
| 4/4 | 120 | 21.56 | 39.60 | 3929.22 | 2431.48 | 35.46 | 0.190 |
| 4/6 | 168 | 21.55 | 39.74 | 3931.98 | 2416.81 | 35.22 | 0.196 |
| 4/9 | 240 | 21.51 | 39.82 | 3943.04 | 2408.51 | 35.12 | 0.202 |
| 4/13 | 336 | 21.47 | 39.90 | 3954.16 | 2400.26 | 35.07 | 0.208 |
| 4/16 | 408 | 21.43 | 39.82 | 3965.35 | 2408.51 | 35.24 | 0.208 |
| 4/18 | 456 | 21.45 | 39.79 | 3959.75 | 2411.61 | 35.27 | 0.205 |
| 4/18 | 468 | 21.45 | 39.78 | 3959.75 | 2412.65 | 35.28 | 0.205 |
| 4/19 | 480 | 21.45 | 39.84 | 3959.75 | 2406.44 | 35.17 | 0.207 |
| 4/19 | 492 | 21.47 | 39.84 | 3954.16 | 2406.44 | 35.12 | 0.206 |
| 4/20 | 504 | 21.45 | 39.84 | 3959.75 | 2406.44 | 35.16 | 0.207 |
| 4/20 | 516 | 21.49 | 39.84 | 3948.59 | 2406.44 | 35.08 | 0.205 |
| 4/21 | 540 | 21.49 | 39.87 | 3948.59 | 2403.34 | 35.04 | 0.206 |
| 4/22 | 564 | 21.49 | 39.87 | 3948.59 | 2403.34 | 35.04 | 0.206 |
| 4/23 | 588 | 21.45 | 39.92 | 3959.75 | 2398.20 | 35.03 | 0.210 |
| 4/25 | 636 | 21.54 | 40.03 | 3934.74 | 2386.97 | 34.67 | 0.209 |
| 4/27 | 684 | 21.48 | 39.98 | 3951.37 | 2392.06 | 34.86 | 0.211 |
| 4/30 | 756 | 21.58 | 39.91 | 3923.72 | 2399.23 | 34.81 | 0.201 |

Table 25 Dynamic test summary for sample J

| Date | Time (hour) | P-wave time (uS) | S-wave time (uS) | P velocity (m/s) | S velocity (m/s) | E (GPa) | v |
|------|------|------|------|------|------|------|------|
| 3/30 | 0 | 21.81 | 40.16 | 3710.74 | 2281.12 | 31.66 | 0.196 |
| 3/30 | 12 | 21.65 | 39.84 | 3752.09 | 2312.45 | 32.49 | 0.194 |
| 3/31 | 24 | 21.65 | 39.92 | 3752.09 | 2304.53 | 32.36 | 0.197 |
| 3/31 | 36 | 21.65 | 40.08 | 3752.09 | 2288.87 | 32.11 | 0.204 |
| 4/1 | 48 | 21.65 | 40.08 | 3752.09 | 2288.87 | 32.11 | 0.204 |
| 4/1 | 60 | 21.65 | 40.08 | 3752.09 | 2288.87 | 32.11 | 0.204 |
| 4/2 | 72 | 21.65 | 40.08 | 3752.09 | 2288.87 | 32.12 | 0.204 |
| 4/4 | 120 | 21.63 | 40.06 | 3757.32 | 2290.82 | 32.19 | 0.204 |
| 4/6 | 168 | 21.63 | 40.06 | 3757.32 | 2290.82 | 32.20 | 0.204 |
| 4/9 | 240 | 21.63 | 40.06 | 3757.32 | 2290.82 | 32.20 | 0.204 |
| 4/13 | 336 | 21.61 | 40.06 | 3762.57 | 2290.82 | 32.24 | 0.205 |
| 4/16 | 408 | 21.63 | 40.07 | 3757.32 | 2289.84 | 32.19 | 0.205 |
| 4/18 | 456 | 21.63 | 40.02 | 3757.32 | 2294.72 | 32.27 | 0.203 |
| 4/18 | 468 | 21.71 | 40.02 | 3736.48 | 2294.72 | 32.05 | 0.197 |
| 4/19 | 480 | 21.79 | 40.02 | 3715.86 | 2294.72 | 31.87 | 0.192 |
| 4/19 | 492 | 21.81 | 40.16 | 3710.74 | 2281.12 | 31.60 | 0.196 |
| 4/20 | 504 | 21.81 | 40.16 | 3710.74 | 2281.12 | 31.58 | 0.196 |
| 4/20 | 516 | 21.81 | 40.16 | 3710.74 | 2281.12 | 31.57 | 0.196 |
| 4/21 | 540 | 21.85 | 40.19 | 3700.55 | 2278.22 | 31.45 | 0.195 |
| 4/22 | 564 | 21.85 | 40.16 | 3700.55 | 2281.12 | 31.48 | 0.194 |
| 4/23 | 588 | 21.81 | 40.08 | 3718.32 | 2293.54 | 31.74 | 0.193 |
| 4/25 | 636 | 21.78 | 40.09 | 3726.02 | 2292.57 | 31.77 | 0.195 |
| 4/27 | 684 | 21.64 | 40.09 | 3762.37 | 2292.57 | 32.01 | 0.205 |
| 4/30 | 756 | 21.70 | 40.17 | 3747.40 | 2285.23 | 31.78 | 0.204 |

The change of P-wave velocity for sample I and sample J were shown in Figure 34.
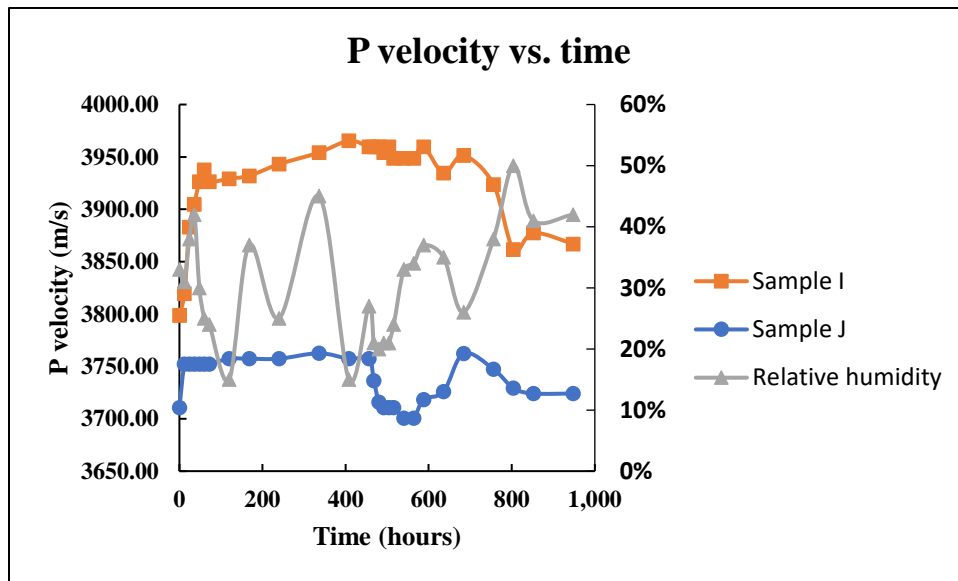


Figure 34 Change of P velocity and relative humidity over time for sample I and sample J and

P-wave velocity increased for sample I at the start of exposure then stabilized due to the contraction of shale sample under appropriate desiccation. P-wave velocity for sample J increased under preservation due to the penetration of preserving fluid. When sample J was taken out of the drilling mud to get exposed after 456 hours, its P-wave velocity started to decrease because of the loss of the penetration fluid. At around 588 hours, sample J's P velocity started to increase again due to the capillary confining effect and contraction of shale samples under continuous loss of moisture content.

The change of S-wave velocity for sample I and sample J is shown in Figure35.
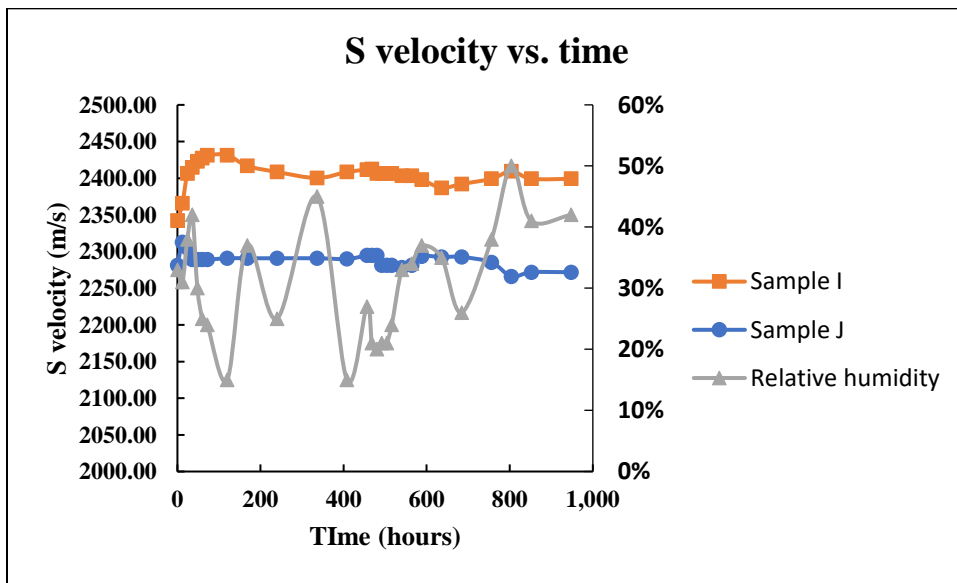


Figure 35 Change of S velocity and relative humidity over time for sample I and sample J

S-wave velocity increased for sample I then stabilized at the start of exposure as the contraction of shale could strengthen samples. S-wave was not affected by the penetration or the loss of drilling mud. Thus, its S-wave velocity stayed stable for sample J while it

was preserved in the drilling mud. Once sample J was taken out of the drilling mud to get exposed, its S-wave velocity still stayed stable.

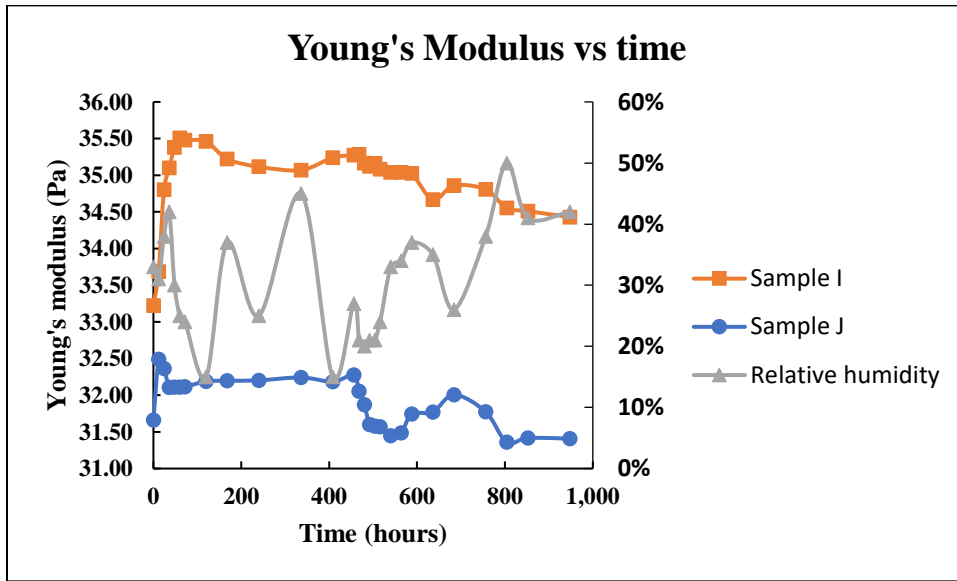The change of Young's modulus for sample I and sample J is shown in Figure 36.



Figure 36 Change of Young's modulus and relative humidity for sample I and sample J over time

Young's modulus increased for both samples. The Young's modulus increased then stabilized for sample J while under preservation due to the incompressibility of penetrated drilling fluid. The incompressibility will lower the shape change under stress. Then, when sample J was taken out of the fluids to get exposed after 456 hours, its Young's modulus began to decrease due to the loss of the penetrated drilling fluid. At around 588 hours, the capillary confining effect dominated the effect which made Young's modulus start to increase again.

The change of Poisson's ratio over time for sample I and sample J is shown in Figure 37.
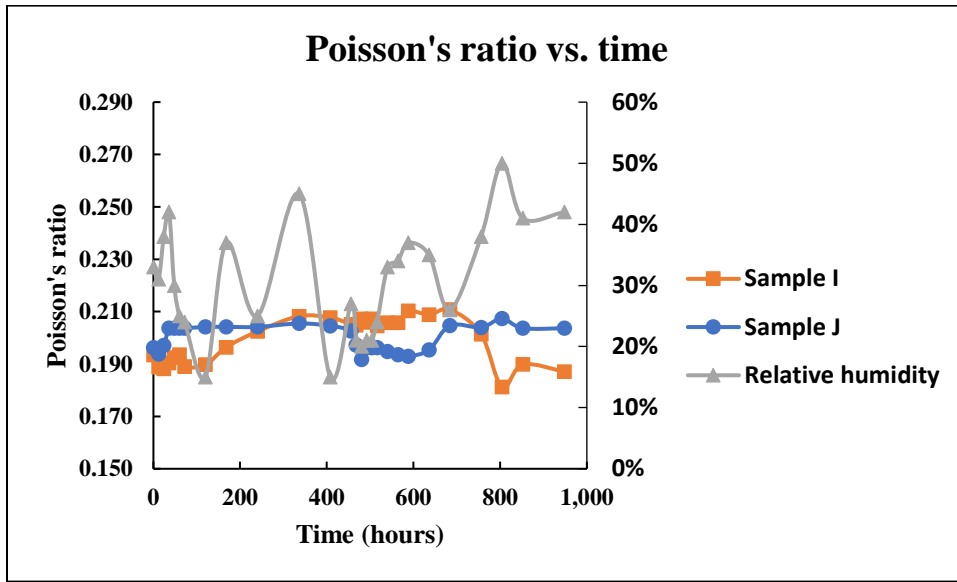
Figure 37 Change of Poisson's ratio and relative humidity over time for sample I and sample J

Poisson's ratio stayed stable for sample I at the start of exposure as the P-wave velocity and S-wave velocity were increasing at a similar rate (Poisson's ratio is calculated by using the ratio between S-wave velocity and P-wave velocity). For sample J, the change of Poisson's ratio was not significant because the change of P-wave velocity was not significant. When sample J was preserved in the drilling mud, its Poisson's ratio increased a little bit because of penetrated drilling mud. When sample J was taken out of fluid to get exposed after 456 hours, its Poisson's ratio began to decrease because of the loss of the penetrated drilling mud. Then at around 588 hours, its Poisson's ratio started to increase again due to the loss of native moisture content which act as a confining effect.

Therefore, Young's modulus and Poisson's ratio change percentage over time for sample I and J can be shown in Figure 32 and Figure 33. The percentage value is calculated

64

relative to the data measured by the first test. Note that the elastic properties are calculated assuming that the theory is still valid for these shales as their saturation changes, and this may not be the case.
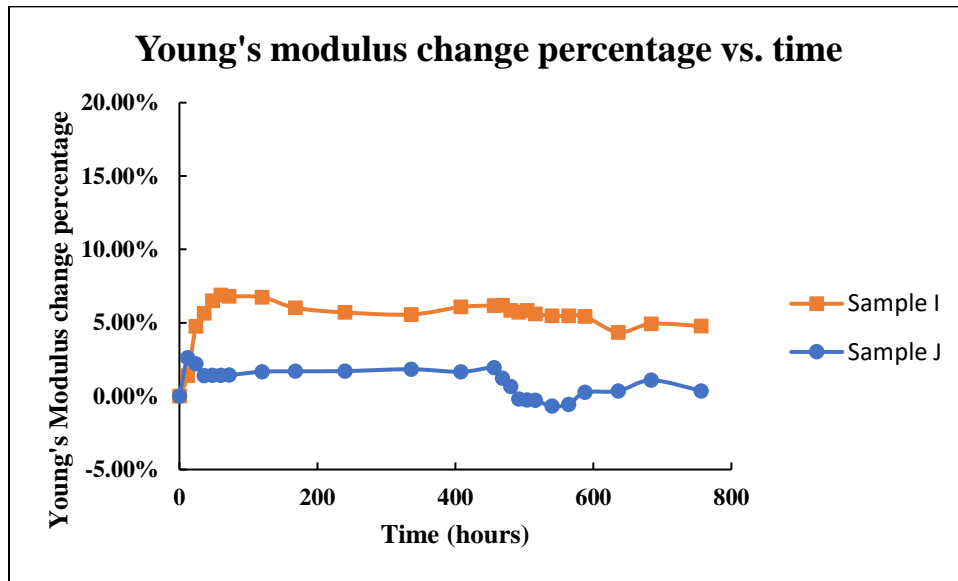


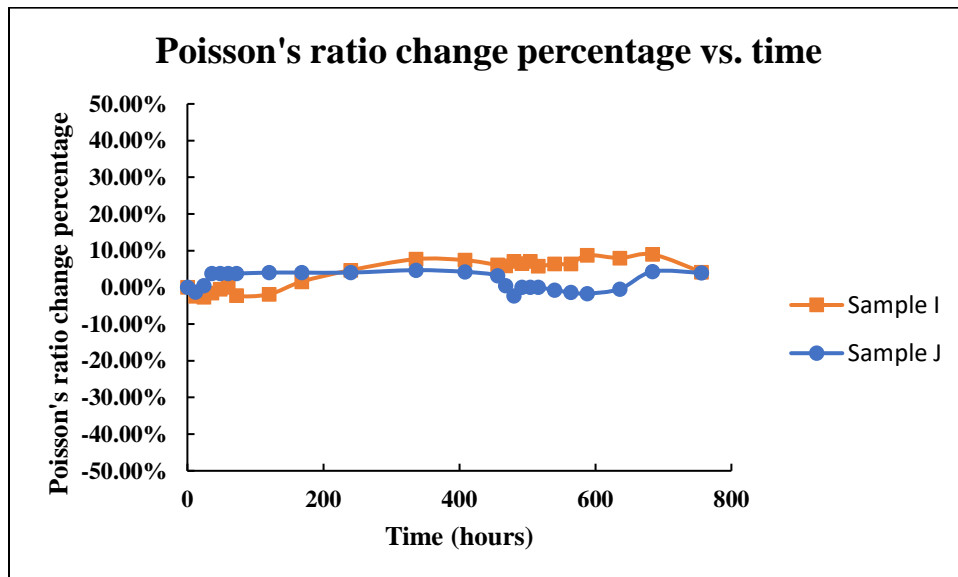Figure 38 Young's modulus change percentage over time for sample I and sample J



Figure 39 Poisson's ratio change percentage over time for sample I and sample J

# Chapter 5. Theoretical Background on dynamic tests, moisture movement and fractures formation

Acoustic velocity measurements are an important way to measure rock dynamic properties without destructing the rock. P-wave can travel through air/liquid while S-wave cannot. The driving forces which caused the movement of the moisture content are discussed below and the sudden drop of P-wave velocity and S-wave velocity can be explained in terms of the formation of fractures due to moisture loss and contraction.

## 5.1 Dynamic Test

The Young's modulus E and Poisson's ratio $\upsilon$ can be calculated by using the formulas below (Frederic L.P., 2007:

$$\nu = \frac{\frac{1}{2} - \left(\frac{V_S}{V_P}\right)^2}{1 - \left(\frac{V_S}{V_P}\right)^2}$$

$$E = \rho \frac{V_P^2 (1 + \upsilon)(1 - 2\upsilon)}{(1 - \upsilon)}$$

As noticed, the Poisson's ratio is directly influenced by the ratio between S-wave velocity and P-wave velocity which indicates that if P-wave and S-wave velocities change at a different ratio, the Poisson's ratio calculated will also change accordingly in the dynamic measurements. The Poisson's ratio variation with the ratio of S-wave and P-wave velocities is shown in the Figure 40. Poisson's ratio decreases with the increase of ratio between S-wave velocity and P-wave velocity. Acoustic velocities are affected by the

material mechanical properties which are related to the mineralogy, porosity, saturation and anisotropy. P-wave and S-wave velocity will be significantly affected by the formation of fractures. P-wave velocity will decrease if there are cracks initiated in the direction which is perpendicular to the wave propagation direction, whereas, S-wave velocity will decrease if there are fractures initiated in the direction which is paralleled with the wave propagation direction (Frederic L.P., 2007).
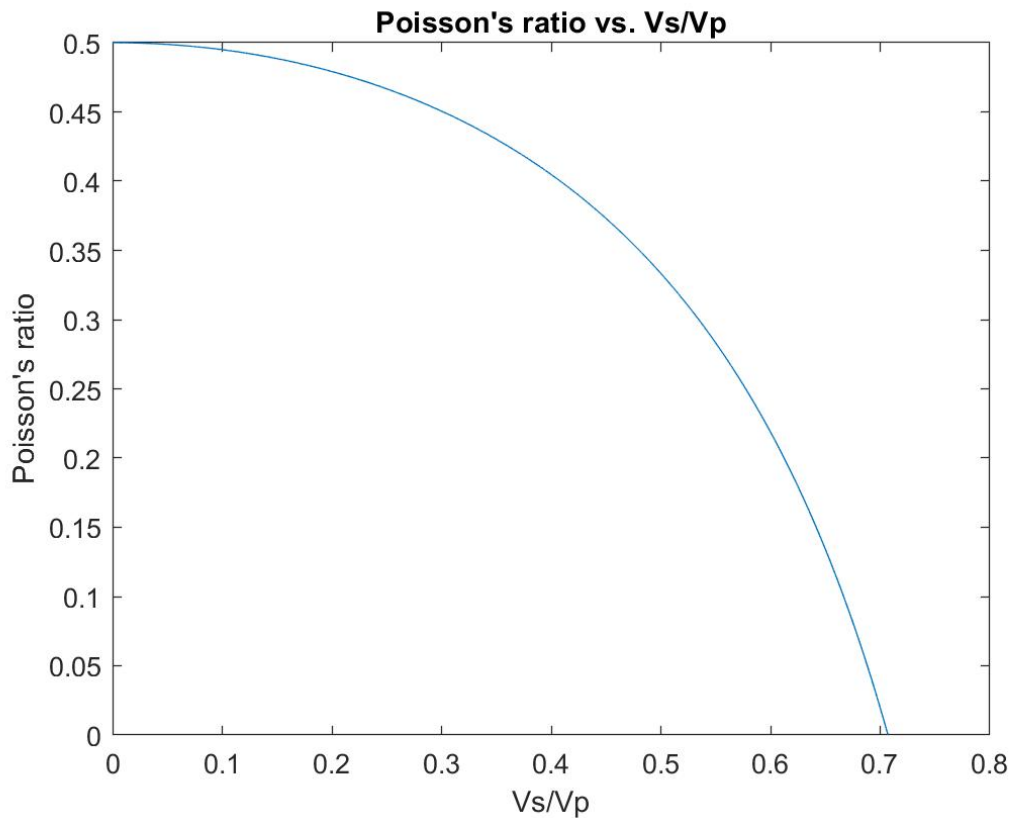


Figure 40 Poisson's ratio and Vs/Vp relationship

Cuxac and Homand (1992) found that the acoustic velocities would increase if the pore was closed. This is due to that the wave velocities transmit faster in the solid than in the

air. Nur and Simmons (1969) found that the growth of cracks would result in the increase of signal attenuation without affecting the propagation velocities.

## 5.2 Driving forces which cause absorption and loss of moisture content

According to Seedsman's (1993) finding, there's a negative electric charge with argillaceous particle which will interact with the interstitial solution. The different ion concentrations between the particles and fluid would induce an osmotic pressure, which adds to the water pressure.

The chemical potential can be described by using the formula below in an open system with different phases of one substance (Nirina R. 2000):

$$\mu_r = \frac{\partial G}{\partial m_r}$$

Where,

$\mu_r = chemical\ potential$

$G = specific\ free\ enthalpy$

$m_r = mass\ per\ reference\ volume\ of\ the\ species\ r$

Mass transfer is decided by chemical potential gradients. The mass transfer only depends on P which leads to Darcy's law for incompressible fluids. The mass transfer only depends on concentration which leads to Fick's law for dilute solutes. This leads to

68

classical mass transferring until the chemical potential equilibrium between air in the lab environment and the moisture content is reached.

Assume an ideal semi-permeable exists between shale and fluid, the osmotic pressure developed between the drilling mud and shale could be determined by the formula below (H. Santos, 1997):

$$\pi = -\frac{RT}{V_w} \ln \frac{p_w}{p^o{}_w}$$

Where,

$V_w = partial\ molar\ volume\ of\ water$

$R = universal\ gas\ constant$

$T = absolute\ temperature$

$p_w = partial\ pressure\ of\ pure\ water\ vapor\ at\ temperature\ T$

$p^o{}_w = partial\ pressure\ of\ pure\ water\ at\ the\ same\ temperature\ T$

While shale is exposed to air, the vapor pressure tends to remain in equilibrium with the capillary pressure (Edward M. and Van E., 1976). The equilibrium would be broken if any of them change. The water pocket in the shale would grow until the equilibrium is reached again if the vapor pressure is greater than the capillary pressure.

## 5.3 Capillary confining effect and contraction of shale due to the moisture loss

The confining effect of the capillary pressure which improves the inter-grains surface with higher adhesion causes the increase of Young's modulus and compressive strength. The attraction forces between them can be described by using the formula and illustration below (Mason and Clark, 1965; Groger et al., 2003).

$$F = 2\pi b\sigma + \pi b^2 P_c$$
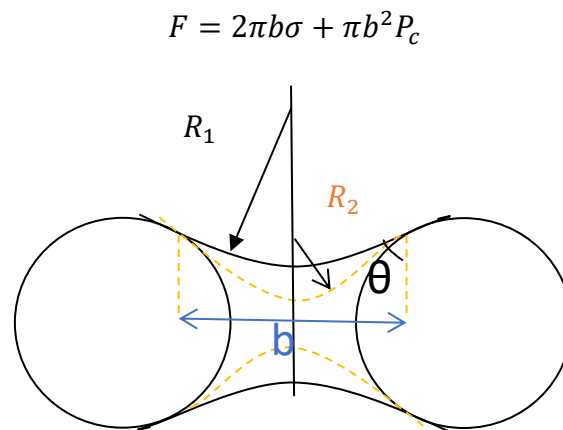


$where\ F = attraction\ force,$

$\sigma = surface\ tension,$

$b = radius\ of\ the\ liquid\ bridge,$

$$Pc = capillary\ pressure = \frac{2\sigma \cos\theta}{R}$$

Due to the loss of the moisture content between the interlayer, the radius between the interlayers is going to decrease. As the radius decreased, the capillary pressure is going to increase which makes the attraction force increase according to the formula above. This force will reinforce shale on one hand. On the other hand, this force can also cause the shrinkage of shale samples and possible cracking Due to the shrinkage of shale samples, the space between the interlayer would be lowered, the P-wave and S-wave velocities both increased.

(Chenevert, 1970) also postulated that for a shale which air was not able to enter through the pore space, the contraction acted like a confining pressure on the shale which strengthens the rock if not excessive.

The P-wave velocity and S-wave velocity would both increase with the shrinkage of the shale as P-wave velocity travel faster in solids and liquid than in air, S-wave can only travel in the solids. The Young's modulus will increase with the contraction of shale too.

F. Valès (2004) conducted an experiment to determine the expansion/contraction of shale during desaturation. He attached two strain gauges in two directions (one is perpendicular to the layer plane, and the other one is parallel to the layer plane). Then he monitored the change of the volume of shale plug during saturation and desaturation. He observed that shale would shrink quite significantly in the direction which was perpendicular to the layer plane during the desaturation process. He concluded this was due to the closing of the interlayer space induced by the loss of moisture content between the interlayers. He

believed that this interlayer space might represent a preferential path for the moisture content loss.

## 5.4 Formation of fractures

There are mainly two reasons for the growth of fractures of exposed sample, e.g., when there is a relative humidity change namely the fracture energy which is required to make the cracks grow would also change accordingly (higher relative humidity will lower the fracture energy); the absorption of moisture content from the lab environment will generate higher capillary pressure.

### 5.4.1 Fracture energy

For a material with cracks, the required tensile stress to make it grow can be described by using the Griffith fracture criterion shown as below (Edward M. and Van E., 1976):

$$\sigma_t = \left(\frac{2E\gamma}{\pi c_0}\right)^{\frac{1}{2}}$$

Where $\sigma_t = tensile\ stress\ necessary\ to\ cause\ crack\ growth,$

$\qquad E = Young's\ modulus$

$\qquad \gamma = surface\ energy$

$\qquad c_0 = one-half\ the\ initial\ flaw\ or\ crack\ length$

The absorption of the moisture decreases the surface energy ($\gamma$) which lowers the tensile stress necessary to cause crack growth (the fracture will be easier to grow) (Edward, V.

M., 1976). If the relative humidity fluctuates, the absorption or loss of the moisture content will happen accordingly (If the relative humidity is higher, the environment's vapor pressure will be higher. As the environment's vapor pressure is higher than the capillary pressure in the samples, the moisture content tends to move from the environment with higher vapor pressure to the environment with lower capillary pressure. If the environment pressure fluctuated, both loss and absorption of moisture content shall happen corresponded with the relative humidity change. Due to the fluctuation of the relative humidity corresponded with the weather change, the water vapor pressure changed in the lab environment. Then, the tensile stress necessary to cause crack growth for a material with crack also changed accordingly. Higher tensile stress would result while the rock is exposed to air (Nirina R. 2000). Therefore, the cracks would tend to grow. As the crack length increases, the tensile stress needed to make the crack grow would also decrease according to the formula shows above. Eventually, the crack would localize due to the growth of cracks along the weakest plane.

## 5.4.2 Capillary tension

Due to the fluctuation of the relative humidity, the water vapor pressure changes in an uncontrolled environment in accordance to the relative humidity change. Therefore, the loss and absorption of moisture will both occur due to the fluctuation of the relative humidity as the moisture content tends to move from the environment with higher pressure to the environment with lower pressure. During this process, some of the air in the room environment will get trapped in the pores. As shown in the sketch below, the air

73

pressure would build up due to the trap of air (water is the wetting phase). Then the

weakest plane tends to fail due to the capillary pressure developed (Schmitt L., 1994).
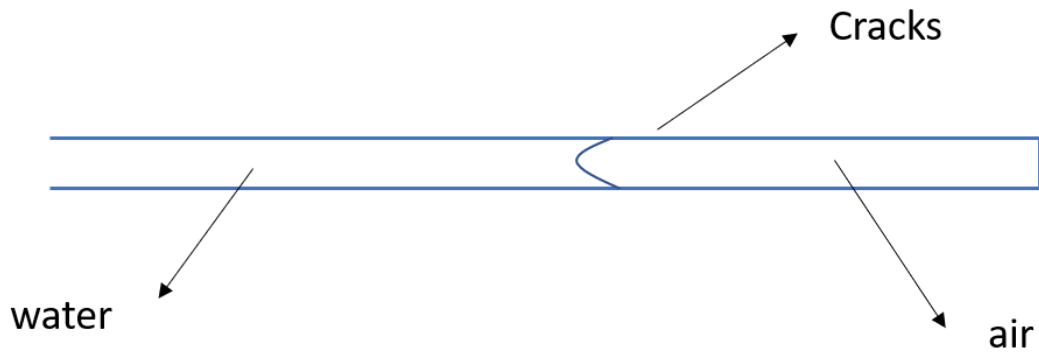


The capillary tension can be calculated by using the equation below:

$$Pc = \frac{2\sigma \cos \theta}{R}$$

Where,

$\sigma = interfacial\ tension\ between\ air\ and\ water\ \left(= 72.75 \times \frac{10^{-3}N}{m}\right)$

$\theta = contact\ angle\ between\ the\ rock\ and\ the\ interface$

$R = raidus\ of\ the\ pore\ throat$

### 5.4.3 Impact of fractures

The growth of micro-cracks would significantly attenuate dynamic signals. Dynamic waves travel faster in solid than in liquid or air. Once the fractures localized, the P-wave and S-wave will suddenly decrease due to the fractures space. Part of the pre-existing cracks are marked in the Figure 41,
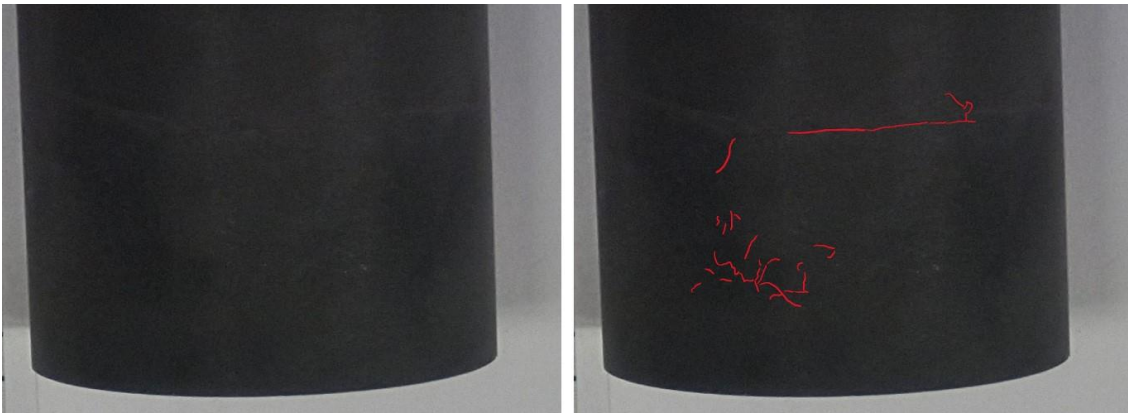


Figure 41 Pre-existing cracks

As the formation of fractures also create more space, Young's modulus and Poisson's ratio will also decrease as the axial displacement would increase under the same stress (Nur and Simmons, 1969).

# Chapter 6. Analysis of the experimental observations

As shown in the well log plot and CT scanning image in Figure 3, the core has many pre-existing small cracks. These cracks represent a major path which fluids could penetrate through. During the drying process, they also became potential structures to form fractures as they are the weakest structure in shale.

## 6.1 Sample B, D, E, F and G analysis

For sample B, D, F and G which were not contacted with any fluids, and tested while they were exposed to air, their P-wave and S-wave velocities increased due to the shrinkage of the shale samples which was also observed by F. Valès (2004). It is observed that the P-wave velocity and S-wave velocity for these samples increased at the start of exposure due to the contraction of shale samples induced by the capillary confining effect. Poisson's ratio is calculated by using the ratio between S-wave velocity and P-wave velocity. It will decrease with the increase of Vs/ Vp ratio.  At the start of exposure, S-wave and P-wave velocity increased at a similar rate. Therefore, the Poisson's ratio stayed stable at the start of exposure according to the relationship between Poison's ratio and Vs/Vp ratio shown in Figure 40. The increase of Young's modulus is likely because by:

The capillary tension which increases the attraction force between the interlayers acting as a confining effect. The attraction force will cause shale samples to contract which will strengthen the rock if the desiccation was not excessive (please refer to section 5.3 for more details).

The sudden drop of P-wave velocity, S-wave velocity, Young's modulus and Poisson's ratio was observed for sample B, D (vertical direction), F, G at 336 hours, 336 hours, 139 hours, 353 hours respectively. The relative humidity shown in Figure 12 was not stable due to the weather change during the test period. As the relative humidity stayed low for a couple of days which generated higher vapor pressure (due to higher relative humidity) than the capillary pressure between the shale interlayers, the absorption of moisture can occur due to this imbalance (Edward M. and Van E., 1976). The absorption and loss of moisture trapped some air between the interlayers (Taylor R. K. and Spears D. A., 1970; Schmitt L., 1994) which made higher tension to develop between the interlayers due to the capillary pressure effect. Therefore, failure would start to develop along the weakest planes, growing micro-cracks. The moisture content also decreased the surface energy. The decreased surface energy lowered the stress required to cause the crack growth according to the Griffith Criterion. Due to all the reasons stated above, the micro-crack was more likely to grow. The increased crack length would decrease the required stress to cause micro-cracks growth thereafter. After some time, the crack formed. The formed crack will significantly lower the P-wave, S-wave velocity (Frederic L.P., 2007), Poisson's ratio and Young's modulus.

Nur and Simmons (1969) found that the growth of the micro-cracks would result in the increase of signal attenuation without affecting the propagation velocities. This is the reason why the dynamic signal in the horizontal direction lost during the test for sample D.

From the well log and CT image, sample E was with the least micros-fissures. It took a longer time for the loss of moisture content to show an impact on sample E's dynamic mechanical properties as the moisture loss might have been confined to the outer surface. That's the reason why sample E's dynamic mechanical properties remained unchanged before 696 hours. The P-wave velocity of sample E decreased at 696 hours due to the loss of the moisture content from the cracks. S-wave velocity increased due to the contraction of shale samples. Young's modulus increased due to the contraction of shale samples and capillary confining effect. Poisson's ratio suddenly decreased as P-wave velocity decreased and S-wave velocity increased (Poisson's ratio is calculated by using the ratio between the P-wave velocity and S-wave velocity).

## 6.2 Sample A and H analysis

Sample H's behavior while in the decane were recorded. While sample H was preserved in the decane: As P-wave velocity travels faster while in the liquid than in the air, the P-wave velocity increased due to penetration of decane through the pre-existing existing cracks. S-wave velocity could not transmit through air or liquid. Therefore, S-wave velocity stayed stable at the start as decane wouldn't impact on S-wave velocity. As the liquid is less compressible than the air, Young's modulus would increase if the decane entered. The Poisson's ratio was calculated by using the ratio between the P-wave velocity and S-wave velocity, the Poisson's ratio likely increased due to the penetration of the decane. The Poisson's ratio decreased at the start of exposure according to the relationship between Poison's ratio and Vs/Vp ratio shown in Figure 40. (with P-wave velocity increased, S-wave velocity remained stable, Vs/Vp ratio decreased).

When sample A and sample H were taken out of the fluid to get exposed, the weight decrease of the sample H was more than its weight gain while under preservation in the decane. The moisture loss during the exposure period consisted of two parts:

1. The loss of fluids which penetrated through pre-existing cracks.

2. The loss of the local moisture content between the interlayer.

The loss of these two types of moisture content would have opposite impacts on the shale dynamic mechanical properties (P-wave velocity, S-wave velocity, Young's modulus, Poisson's ratio):

The loss of the fluids which penetrated through pre-existing cracks would decrease the P-wave velocity as it travels faster in the liquid than in air. However, this loss wouldn't impact the S-wave velocity as it cannot travel through air or liquid. Young's modulus would decrease with the loss of the fluids in the pre-existing cracks because of the loss of fluids' incompressibility. The Poisson's ratio would decrease with the loss of the fluids existed in the pre-existing cracks because the Poisson's ratio was calculated by using the ratio between P-wave velocity and S-wave velocity (P-wave velocity would decrease, S-wave velocity would remain stable due to the loss of the fluids in the pre-existing cracks).

The loss of the native fluids existed between the interlayers would tend to strengthen the shale samples due to the capillary confining effect, if the loss is not excessive. P-wave velocity and S-wave velocity would increase due to the contraction of shale samples. Else they would decrease due to desiccation of the rock.

While during early exposure, the fluids in the pre-existing cracks dominated the effect. That's why P-wave velocity decreased, S-wave velocity remained stable, Young's modulus decreased, Poisson's ratio remained stable while at the start of exposure for sample A and sample H.

The sudden drop of P-wave velocity, S-wave velocity, Young's modulus and Poisson's ratio were observed for sample A and sample H at 600 hours and 403 hours. The relative humidity shown in Figure 12 was not stable due to the weather change during the test period. As the relative humidity remained low for a couple of days, it generated higher vapor pressure (due to higher relative humidity) than the capillary pressure between the shale interlayers. Thus, the absorption of moisture content can be observed due to this imbalance (Edward M. and Van E., 1976). The absorption and loss of moisture trapped some air between the interlayers (Taylor R. K. and Spears D. A., 1970, Schmitt L., 1994) which made higher tension stress developed between the interlayers due to the capillary pressure effect. The failure would start to get developed along the weakest plane because of the higher tension stress. The micro-cracks began to grow. The moisture content absorbed also decreased the surface energy. The decreased surface energy lowered the stress required to cause the crack growth according to the Griffith Criterion. Due to all the reasons stated above, the micro-cracks started to grow. The increased crack length will decrease the required stress to cause micro-cracks growth thereafter. After some time, the crack formed. The formed crack will significantly lower the P-wave, S-wave velocity (Frederic L.P., 2007), Poisson's ratio and Young's modulus.

## 6.3 Sample I and J analysis

For sample I which was not contacted with any fluids, and tested only while it was exposed to air, its P-wave and S-wave velocities increased due to the shrinkage of the shale samples which was also proved by F. Valès (2004). It is observed that the P-wave velocity and S-wave velocity for sample I were increasing at a similar rate. This is the reason why Poisson's ratio remained stable as it is calculated by using the ratio between P-wave velocity and S-wave velocity according to the relationship between Poison's ratio and Vs/Vp ratio shown in Figure 40. The increase of the Young's modulus is because:

The capillary tension which increases the attraction force between the interlayers acting as a confining effect. The increase of attraction will also make shale shrink (please refer to section 5.3 for more details).

While sample J was preserved in the drilling mud: As P-wave velocity travels faster while in the liquid than in the air, the P-wave velocity increased due to penetration of drilling mud through the pre-existing cracks powered by the osmotic pressure. S-wave velocity could not transmit through air or liquid. Therefore, S-wave velocity stayed stable as drilling mud wouldn't impact on S-wave velocity. As the fluid has much larger compressibility than the air, the Young's modulus would increase because of the drilling mud entered. The Poisson's ratio was calculated by using the ratio between the P-wave velocity and S-wave velocity, the Poisson's ratio increased due to the penetration of the drilling mud (with P-wave velocity increased, S-wave velocity remained stable).

While sample J was taken out of the fluid to get exposed: As the weight of sample J decreased is more than the weight it gained while under preservation in the drilling mud, the moisture loss during the exposure consisted of two parts:

1. The loss of fluids which penetrated through pre-existing cracks.

2. The loss of the local moisture content between the interlayer.

The loss of these two types of moisture content would impose opposite impacts on the shale dynamic mechanical properties (P-wave velocity, S-wave velocity, Young's modulus, Poisson's ratio):

The loss of the fluids which penetrated through pre-existing cracks would decrease P-wave velocity as P-wave velocity travels faster in the liquid than in air. However, this loss wouldn't impact S-wave velocity as S-wave velocity cannot travel through air or liquid. Young's modulus would decrease with the loss of the fluids existed in the pre-existing cracks because of the fluid's incompressibility. The Poisson's ratio would decrease with the loss of the fluids existed in the pre-existing cracks because the Poisson's ratio was calculated by using the ratio between P-wave velocity and S-wave velocity (P-wave velocity would decrease, S-wave velocity would remain stable due to the loss of the fluids existed in the pre-existing cracks).

The loss of the fluids existed between the interlayers would strengthen the shale samples because:

The capillary tension which increases the attraction force between the interlayers acting as a confining effect. The increase of attraction force would also cause the shrinkage of shale samples (please refer to section 5.3 for more details).

P-wave velocity and S-wave velocity would increase due to the contraction of shale samples.

While exposing, the fluids in samples' pre-existing cracks dominated the effect. That is why P-wave velocity decreased, S-wave velocity remained stable, Young's modulus decreased, Poisson's ratio remained stable for sample J.

At around 588 hours, the relative humidity increased due to the rainy weather. The vapor pressure also increased corresponded with the relative humidity change. The moisture content began to get into the shale samples which increased P-wave velocity as P-wave travels faster in the fluid. S-wave stayed stable as the fluid has no impact on S-wave velocity. Young's modulus increased due to fluid's compressibility. Poisson's ratio increased as it is calculated by using the ratio between the P-wave velocity and S-wave velocity (with P-wave velocity increased, S-wave velocity unchanged).

# Chapter 7. Conclusion:

1. Chemical potential and hydration potential (difference between vapor pressure in the lab environment and capillary pressure between the interlayers) are the main driving force for the moisture content movement. The absorption of moisture happens while the vapor pressure is higher than the capillary pressure within the shale interlayers. The loss of moisture content happens while the capillary pressure is higher than the vapor pressure.

2. Shale's strength will increase (due to closure of pore space and the increase of capillary confining effect due to the loss of moisture content) during exposure if the exposure is not excessive as to cause excessive shrinkage

3. Poisson's ratio did not show change due to the contraction of shale during the loss of native moisture content as the P-wave velocity and S-wave velocities increased at a similar rate due to the contraction of shale during the loss of native moisture content at the start of exposure.

4. The penetration of preserving fluid will increase shale's dynamic Poisson's ratio. P-wave velocity will increase in response to the absorption of preserving fluid since the P-wave travels faster in liquid than in air. S-wave velocity is not affected by the absorption of preserving fluid since it cannot travel through liquid and air.

5. The growth of the micro-cracks will attenuate dynamic signals.

6. The formation of fractures will significantly decrease the dynamic P-wave velocity and S-wave velocity.

7. While shale is exposed for a longer time periods, fractures localized due to the capillary pressure built (air were trapped inside shale due to the alteration between absorption and loss of moisture content).

# Reference

1. Aadnoy, B.S. 1988. Modeling of the Stability of Highly Inclined Boreholes in Anisotropic Rock Formations (includes associated papers 19213 and 19886). SPE Drill Eng 3 (3): 259-268. SPE-16526-PA. http://dx.doi.org/10.2118/16526-PA.

2. Ahmad, G., Zamora M., Cosenza P., Effects of desiccation on the elastic wave velocities of clay-rocks. International Journal of Rock Mechanics & Mining Sciences, 2009

3. Akrad, O.M., Miskimins, J.L., and Prasad, M.. 2011. The Effects of Fracturing Fluids on Shale Rock Mechanical Properties and Proppant Embedment. Paper SPE-146658-MS presented at SPE Annual Technical Conference and Exhibition, October 30 – November 2, 2011, Denver, Colorado, USA.

4. Bourgoyne Jr., A. T., Millheim, K. K., Chenevert, M. E., & Young Jr. F. S. (1991). Applied Drilling Engineering, Second Printing, Society of Petroleum Engineers, Richardson, TX.

5. Carol Tosaya & Amos Nur, Effects of Diagenesis and clays on Compressional Velocities in Rocks, Geophysics Research Letters, Vol. 9, No. 1, Page 5-8, January 1982

6. Chenevert M. E. Absorptive pore pressures of argillaceous rocks in Rock Mechanics – Theory and Practice, Eleventh Symp. Rock Mech, A.I.M.E. (Ed. By Somerton) pp 599-627 (1970)

7. Darley, H. C. H. & Gray, G. R. (1991). "Composition and properties of drilling and completion fluids", Fifth Edition, Houston, Texas: Gulf Publishing Company.

8. Derjguin, B., Churaev, N. 1978. On the question of determining the concept of disjoining pressure and its role in the equilibrium and flow of thin films. Journal of Colloid and Interface Science 66(3).

9. Diane L. J., Mechanical and Acoustical Properties of Sandstones and Shales, A dissertation submitted to the Department of Geophysics, Stanford University, March 1991

10. Dong F., Xiangfang L., Xiangzeng W., Jing L., Fengrui S., Zheng Z., Tao Z., Peihuan L., Yu C., Xu Z., Water absorption and its impact on the pore structure characteristics of shale clay, Applied Clay Science 155 (2018) 126-138

11. EDWARD, M., V.E., The Mechanisms of Strength Reduction due to Moisture in Coal Mine shales, Int. J. Rock Mech. Min, Sci. & Geomech. Abstr. Vol. 13, pp.61-67, Pergamon Press 1976.

12. F. Valès, D. Nguyen Minh, H. Gharbi, A. Rejeb, Experimental study of the influence of the degree of saturation on physical and mechanical properties in Tournemire shale (France), Applied Clay Science 26 (2004) 197-207, April 2, 2004

13. Fjaer, E. et al. 1992. Petroleum Related Rock Mechanics, 1-338. Amsterdam: Developments in Petroleum Science No. 33, Elsevier, Amsterdam.

14. Forsans, T. M. & Schmitt, L. (1994). "Capillary forces: the neglected factor in shale instability studies?, " Eurock '94 Symp., Proc. Balkema, Rotterdam.

15. Frederic, L.P., Geraldine, F., Damage Evaluation with P-Wave Velocity Measurements during Uniaxial Compression Tests on Argillaceous Rocks. International Journal of Geomechanics, 2007, 7(6): 431-436

16. Groger, T., Tuzun, U., Heyes, D. M., 2003. Modeling and Measuring of Cohesion in Wet Granular Materials. Powder Technology 133 (2003) 203-215

17. H. Santos, A New Conceptual Approach to shale Stability, Dissertation Approved for the University of Oklahoma Mewbourne School of Petroleum and Geological Engineering. University of Oklahoma, 1997.

18. Hale, A. H. & Mody, F. K. (1992). "Experimental investigation of the influence of chemical potential on wellbore stability." IADC/SPE Drilling Conference, New Orleans, Paper IADC/SPE 23885.

19. J. M. Kate, Influence of Saturation on Dynamic Elastic Constants of Sandstones, Datta Meghe Institute of Engineering, Technology & Research, Wardha, 442004, India

20. J. W. Devilbiss, J. R. Bulau, B. R. Tittmann, R. J. Meyer, Dependence of Attenuation on Water Saturation in a Porous Carbonate Rock, Gulf R&D

21. Lai, B.T., Li, H., Zhang, J.L., Jacobi, D., Georgi, D. Water Content Effects on Dynamic Elastic Properties of Organic-Rich Shale. Paper SPE-175040-MS

presented at the SPE Annual Technical Conference and Exhibition, September 2015, Houston, Texas, USA

22. Lin S., SPE, and B. Lai, Experimental Investigation of Water Saturation Effects on Barnett Shale's Geomechanical Behaviors, Paper SPE 166234 at the SPE Annual Technical Conference and Exhibition held in New Orleans, Louisiana, USA, 30 September–2 October 2013.

23. M., Gasc-Barbier, D., Tessier Structural Modifications of a Hard Deep Clayey Rock due to Hygro-Mechanical Solicitations, 10.1061/ (ASCE)1532-3641(2007):3(227)

24. Mikaël, R. d. S., Christian, S., Jean-Claude V. Unsaturated rock mechanics applied to a low-porosity shale. Avenue F. D. Roosevelt, 50 CP 194/2, 1050 Bruxelles, Belgium, 27 January 2007

25. N., Ramambasoa, D., Nguyen Minh, A., Rejeb, Hydromechanical behavior of shales – Application to the Tournemire site, France, Pacific Rocks 2000, Girard, Liebman, Breeds & Doe (eds) O 2000 Balkema, Rotterdam, ISBN 90 5809 155 4

26. Nur, A. and Simmons, G., Stress induced velocity anisotropy in rock: An experimental study. J. Geophys. Res., 74, 667-674, 1969

27. Onaisi, A. Durand, C. & Audibert, A. (1994). "Role of hydration state of sahles in borehole stability studies," Eurock '94, Prooc., pp. 275-284, Balkema, Rotterdam.

28. PHAM, Q.T., VALES, F., MALINSKY, L., NGUYEN MINH, D. and GHARBI, H., Effect of desaturation-resaturation on mechanical behaviour of shale, Paper

ARMA/USRMS 05-793 presented at the 40th U.S. Symposium on Rock Mechanics (USRMS): Rock Mechanics for Energy, Mineral and Infrastructure Development in the Northern Regions, held in Anchorage, Alaska, June 25-29, 2005.

29. Philippe C., Ahmad G., Nicolas F., ANDRÉ R., Effects of Drying on the Low-frequency Electrical Properties of Tournemire Argillites, Pure appl. Geophys. 164 (2007) 2043-2066

30. Russ Ewy, 2014, Shale Handling, Preservation and Sampling, 3$^{rd}$ Workshop on Petroleum Geomechanics Testing, Minneapolis, 31 May 2014

31. Schmitt, L., Forsans, T. & Santarelli, F. J. (1994). "Shale testing and capillary phenomena", Int. J. Rock Mech. Min. Sci. & Geochem. Abstr., 31, pp. 411-427.

32. Seesman, W. 1993. Characterizing clay shales. In J. Hudson (Ed.), Comprehensive Rock Engineering. Pergamon Press.

33. Taylor R. K. & Spears D. A. The breakdown of British coal measure rocks, Int. J. Rock Mech. Sci. 7. 481-501 (1970)

34. Younane A., Minh T., Son H., Christopher B., Alberto O., Franz-Josef U., Geomechanics Field and Laboratory Characterization of Woodford Shale, 2007 SPE Annual Technical Conference and Exhibition, 11-14 November 2007, Anaheim, California, U. S. A.

35. Yu Weiqi, Laboratory Geomechanical Characterization of the Arbuckle Group and Crystalline Basement Rocks in Oklahoma, Thesis Approved for the

University of Oklahoma Mewbourne School of Petroleum and Geological Engineering. University of Oklahoma, 2017.

36. Zimmer, M. A., Prasad, M., and Nur, A., 2002a, Laboratory P- and S-wave measurements on sands: Implications for pressure trends: Expanded Abstracts of the Environmental Problems (SAGEEP), Las Vegas, NV, February 9-13, 2002, Environmental and Engineering Geophysical Society, Wheat Ridge, CO.

# Appendix

The measurement error for the dynamic test and weight measurement are shown in the

table below.

Table 26 Measurement error

| Measurements | error |
|---|---|
| P-wave velocity | 2% |
| S-wave velocity | 4% |
| Weight | ±0.1 g |